IEEE Access
Multidisciplinary | Rapid Review | Open Access Journal

Received June 3, 2021, accepted June 18, 2021, date of publication June 22, 2021, date of current version June 30, 2021.

*Digital Object Identifier 10.1109/ACCESS.2021.3091479*

# Metamaterial-Inspired Antennas: A Review of the State of the Art and Future Design Challenges

**CHRISTOS MILIAS[1,4], RASMUS B. ANDERSEN[1], PAVLOS I. LAZARIDIS[2], (Senior Member, IEEE), ZAHARIAS D. ZAHARIS[3], (Senior Member, IEEE), BILAL MUHAMMAD[4], JES T. B. KRISTENSEN[1], ALBENA MIHOVSKA[4], (Member, IEEE), AND DAN D. S. HERMANSEN[1]**

[1]MyDefence ApS, 9400 Nørressundby, Denmark
[2]School of Computing and Engineering, University of Huddersfield, Huddersfield HD1 3DH, U.K.
[3]Department of Electrical and Computer Engineering, Aristotle University of Thessaloniki, 541 24 Thessaloniki, Greece
[4]Department of Business Development and Technology (BTECH), Aarhus University, 8000 Aarhus, Denmark

Corresponding author: Christos Milias (cm@mydefence.dk)

This work was supported by the Project MObility and Training fOR beyond 5G ecosystems (MOTOR5G) through the European Union's Horizon 2020 Programme of the Marie Skłodowska-Curie Actions (MSCA) Innovative Training Network (ITN) under Grant 861219.

**ABSTRACT** Metamaterials are artificial structures with the ability of exhibiting unusual and exotic electromagnetic properties such as the realisation of negative permittivity and permeability. Due to their unique characteristics, metamaterials have drawn broad interest and are considered to be a promising solution for improving the performance and overcoming the limitations of microwave components and especially antennas. This paper presents a detailed review of the most recent advancements associated with the design of metamaterial-based antennas. A brief introduction to the theory of metamaterials is provided in order to gain an insight into their working principle. Furthermore, the current state-of-the-art regarding antenna miniaturisation, gain and isolation enhancement with metamaterials is investigated. Emphasis is primarily placed on practical metamaterial antenna applications that outperform conventional methods and are anticipated to play an active role in future wireless communications. The paper also presents and discusses various design challenges that demand further research and development efforts.

**INDEX TERMS** Metamaterials, electrically small antennas, gain enhancement, isolation enhancement.

## I. INTRODUCTION

Antennas provide the wireless transmission and reception of electromagnetic signals and play an essential role in modern telecommunications. The latest wireless technologies such as the upcoming 5G networks and IoT (Internet of Things) represent the vessel for the establishment of a new era with advanced connectivity. As the demand for higher data rates, reliable communication links, and compact high-performance transceivers booms, the antennas have to adapt and satisfy the ever-increasing requirements. Modern antennas shall have small size, low-profile and high bandwidth, while the radiation pattern and gain should also be sufficient. In parallel, multi-antenna technologies such as massive MIMO and beamforming arrays set additional antenna design challenges [1], [2]. For instance, isolation between neighbouring elements and beamsteering capability are often desired or necessary characteristics for maintaining good performance. Hence, the design of antenna systems becomes highly complicated, especially as the number of elements increases.

Generally, antennas consist of a combination of conductors, dielectrics and other conventional materials that have a certain geometry. Their design follows either traditional analytical methods or rules of thumb that rely on experience [3]. Meanwhile, artificial intelligence and powerful optimization techniques assisted by full-wave simulations are also utilized to obtain the highest possible performance by fine-tuning the structure's parameters [4], [5]. It is obvious that the antenna design is primarily focused on determining the optimum geometrical shape of conventional materials and thus it is bound by the material characteristics. In an effort to overcome

The associate editor coordinating the review of this manuscript and approving it for publication was Chinmoy Saha.

this limitation, metamaterials with their unique properties have gained focus. Despite the fact that metamaterials are microscopically composed of conventional materials (conductors and dielectrics), their macroscopic characteristics are completely different due to their smart shapes. The realisation of negative constitutive parameters in the microwave regime is feasible with metamaterials, while their subwavelength size is another beneficial feature. As a result, the integration of metamaterials into antennas can offer advanced flexibility and enable novel design strategies. Hence, the investigation of the benefits of metamaterial-inspired antennas and their capability of having an active role in modern wireless communications is of great significance.

In this communication, the background of metamaterials is firstly introduced and includes their categorisation, principles of operation and examples of practical implementation. After this, a detailed state-of-the-art investigation regarding metamaterial antennas is presented. Emphasis is placed on three typical metamaterial-inspired antenna design techniques: antenna miniaturisation with metaresonators, gain enhancement, decoupling of antennas placed in vicinity. Antenna miniaturisation is of great importance for shrinking the dimensions of mobile, airborne, wearable and IoT devices, where space limitations prohibit the usage of large antennas, while metamaterial-based small antennas are also envisioned for usage in 6G networks [6]. Here, electrically small antennas loaded with metaresonators are examined in detail and their drawbacks and benefits are highlighted. Gain enhancement is essential for range extension of point-to-point communication links, signal-to-noise ratio (SNR) improvement and interference mitigation. For this reason, metasurfaces that focus electromagnetic radiation and increase the gain of antennas are presented. Furthermore, given the ever increasing number of antennas per communication device, antenna isolation is crucial for minimizing the coupling that mitigates the performance of the multi-antenna system. Therefore, metamaterial decoupling solutions are described and compared in detail. It should be pointed out that works associated with the concept of dynamic metasurface antennas (DMA), which provide beamsteering with lower hardware complexity than conventional phased arrays are not included in this study and the interested reader is referred to [7], [8].

This article aims at shedding light on novel metamaterial antennas that emerged over the last few years, as well as examining their working principles, advantages and disadvantages. In contrast to previous reviews that exclusively focused on metamaterial decoupling methods [9] and metamaterial antennas [10], we provide additional valuable comments on the performance and design techniques. Hence, this review acts not only as a state-of-the-art survey but also as a design guideline that takes into account the theoretical principles and practical limitations and highlights the best designs of the literature. In particular, the main contributions of this paper are as follows,

- Detailed analysis of the state-of-the-art theory and practical design of metamaterial antennas. Here, some theoretical approaches of metamaterial-based antennas are initially studied and their connection to practical implementations and limitations is established.
- Fruitful comparisons between metamaterial-based and conventional designs highlight the strength and weaknesses of each category.
- A brief design methodology regarding antenna decoupling is extracted and provided to the reader.
- Research gaps and challenges associated with the aforementioned metamaterial antenna design methods are identified and future directions are proposed.

The rest of this paper is organized as follows. In Section II, the theoretical background and the fundamental principles of metamaterials are introduced. The latest advancements in metamaterial-based antenna miniaturisation, gain and isolation enhancement are presented in Section III. Section IV presents the future research challenges, while Section V draws some conclusions.

## II. THEORETICAL BACKGROUND

Metamaterials are engineered, man-made materials that are able of manipulating electromagnetic waves in a different way than conventional, natural materials. For instance, structures that exhibit negative permittivity: $\epsilon < 0$ and permeability: $\mu < 0$, are common examples of metamaterials [11]. Three main metamaterial categories can be identified: i) SNG (Single-Negative) metamaterials that possess either negative permittivity (Epsilon-Negative) or negative permeability (Mu-Negative), ii) DNG (Double-Negative) metamaterials that simultaneously have negative permittivity and permeability and iii) ZIM (zero-index materials) that have either zero permittivity or zero permeability. Meanwhile, EBG (Electromagnetic Bandgaps that prohibit the propagation of EM waves) and AMC (Artificial Magnetic Conductors that have zero magnetic field) are also usually regarded as metamaterials. In 1968, Veselago was the first one to theoretically study the electrodynamics of DNG media and pointed out their interesting properties such as reversal of the doppler effect, negative index of refraction $n < 0$ and left-handed propagation [12]. While the conventional materials support the typical forward-wave propagation, the wave in SNG media is evanescent since the propagation constant is real ($\gamma \in \mathbb{R}$). Left-handed or DNG media support backward-wave propagation, where the phase velocity and group velocity are opposite to each other ($v_g v_p < 0$) and the wave travels antiparallel to the power flux.

The realisation of negative permittivity in the microwave regime is possible with a periodic arrangement of thin metallic wires of diameter $\alpha$ and periodicity $p$ as shown in Fig.1 and was initially proposed by Sir John Pendry and his group [13]. This structure is the counterpart of plasmas in lower frequencies and its effective permittivity for an incident electric field parallel to the wires follows a typical Drude behaviour:

$$\epsilon_{eff}(\omega) = 1 - \frac{\omega_p^2}{\omega(\omega + j\omega_c)}, \tag{1}$$

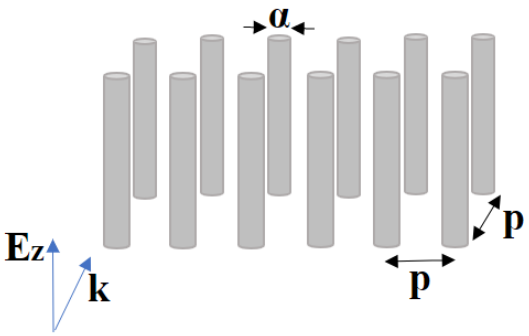


**FIGURE 1.** Periodic arrangement of thin conductive wires for the realisation of negative permittivity.

where $\omega_p$ is the plasma frequency:

$$\omega_p^2 = \frac{2\pi c^2}{p^2 ln(\frac{p}{\alpha})} \tag{2}$$

and $\omega_c$ is the dumping frequency. As depicted in Fig.2, the real part of the effective permittivity is negative below the plasma frequency and the medium can be characterized as ENG.

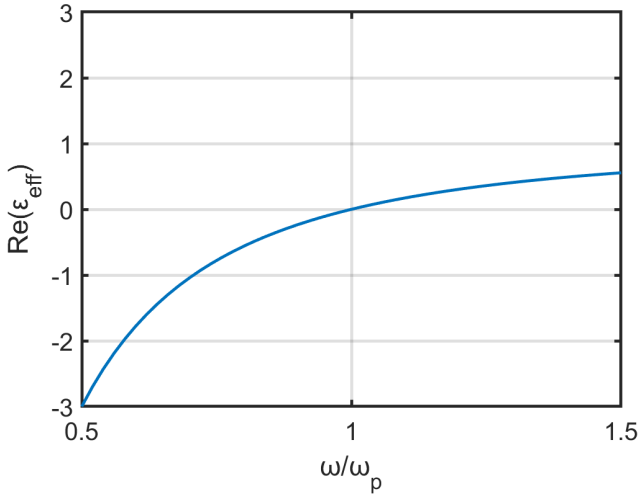


**FIGURE 2.** Real part of the effective permittivity of periodically arranged infinitely long thin wires.

It is well known that there are no materials in nature with negative permeability. Subsequently, it was Pendry again who proposed a Split Ring Resonator (SRR) as depicted in Fig.3, which presents a negative permeability behaviour around its resonance frequency [14]. Under the presence of an external time-varying magnetic field perpendicular to the SRR's surface, currents are induced on both the conductive inner and outer rings and charges are accumulated across the gaps between them. Moreover, SRRs are subwavelength resonators and their size is typically $\lambda/10$. Hence they can be described by an equivalent quasi-static LC circuit and their

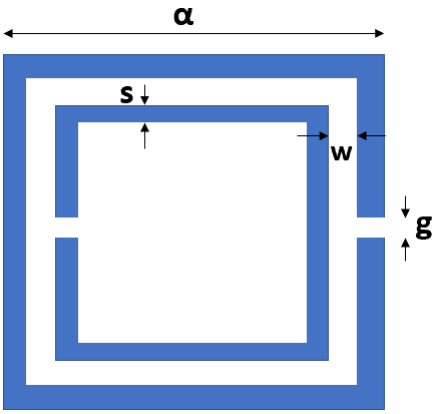


**FIGURE 3.** Geometry of a Square Split Ring Resonator unit cell. Blue parts depict metallization.

resonance frequency $f_0$ is [15], [16]:

$$f_0 = \frac{1}{2\pi\sqrt{LC}} \tag{3}$$

where $L$ is the inductance of the rings and $C$ is the capacitance between them.

In addition, their effective permeability is given by:

$$\mu_{eff}(\omega) = 1 - \frac{A\omega^2}{\omega^2 - \omega_m^2 + j\omega\Gamma_m} \tag{4}$$

where $A$ and $\Gamma_m$ are functions of the geometric parameters $l$, $g$, $s$, $w$ and $\omega_m$ is the resonance frequency. As Fig.4 illustrates, the SRR exhibits a narrow-band resonance where its real permeability is negative. It should be noted that a single SRR or thin wire cell is equivalent to an atom in conventional materials. Hence, in order to create an effective macroscopic ENG or MNG behaviour, a number of periodically arranged thin wires or SRRs is required. Some variations of split-ring resonators or metamaterial unit cells are the open split ring resonators (O-SRRs) [17] and the broadside coupled split-ring resonators (BC-SRRs) [18]. Moreover, the complementary split ring resonator (CSRR) is utilized in many applications [19]. The CSRR is the dual counterpart of the SRR where the SRR's metalization is replaced by air/dielectric and vice versa. Therefore, the babinet's principle can be applied and this is the reason that the CSRR has a similar resonance, but possesses negative permittivity and is excited by a perpendicular electric field [20]. A rigorous analysis regarding the anisotropy and theoretical principles of SRRs and CSRRs can be found in [21], [22]. Finally, other common metamaterials are the omega cells [23], S-shaped cells [24] and resonant electric (ELC) cells [25].

As far as DNG metamaterials, they can be synthesized by combinations of ENG and MNG layers. The experimental demonstration of such a unique material was first accomplished by Smith *et al.* [26] in 2000 using a composite structure consisting of wires and SRRs, which is depicted in Fig.5. Here, the resonant frequency of the SRRs is properly tuned to be lower than the plasma frequency of the thin wires and

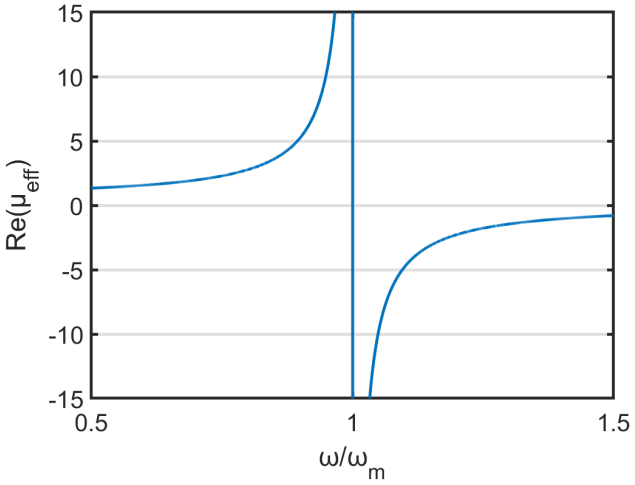


**FIGURE 4.** Real part of the SRR's effective permeability.

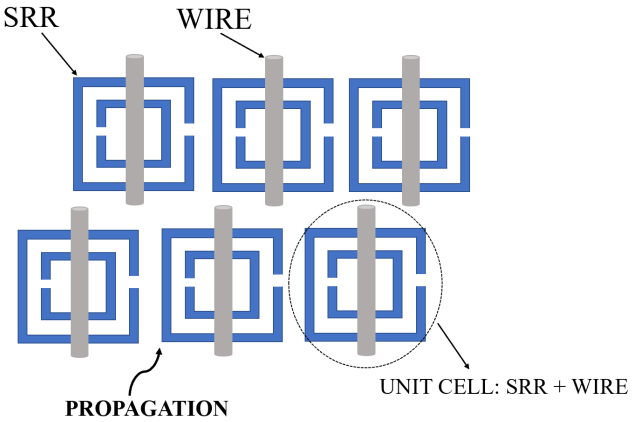


**FIGURE 5.** DNG medium consisting of unit cells that are synthesized by wires (ENG) placed in front of SRRs (MNG) [26]. Both blue and grey parts depict metallization.

thus negative permittivity and permeability are accomplished simultaneously.

An alternative solution for synthesizing a DNG or Left-handed (LH) medium arises from the transmission line (TL) theory. Since the aforementioned metamaterial cells (e.g. SRRs, CSRRs) have subwavelength size, they exhibit high loss, narrowband performance and might be unsuitable for integration with other microwave components. For this reason, several researchers turned to a metamaterial TL approach [27]–[29]. The unit cell of a conventional, right-handed (RH) TL consists of a series inductor $L_R$ and a shunt capacitor $C_R$, when the loss of dielectrics and conductors (equivalent to shunt admittance and series resistance) is neglected. By introducing an additional shunt inductance $L_L$ and series capacitance $C_L$, as shown in Fig. 6, the dispersion characteristics are alternated and this type of TLs is referred as composite right/left handed (CRLH) TL [30]. This becomes apparent by observing the TL's propagation constant: $\gamma = \alpha + j\beta = \sqrt{Z_{cell}Y_{cell}}$, where $Z_{cell}$, $Y_{cell}$ are the equivalent impedance and admittance of the unit cell shown

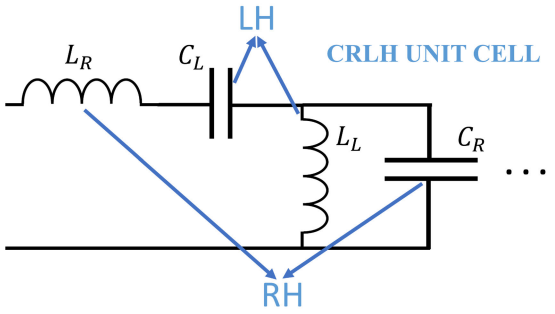


**FIGURE 6.** Unit cell of a Composite Right/Left-Handed Transmission line consisting of series inductor and shunt capacitor (RH) and series capacitor and shunt inductor (LH).

in Fig.6 and are given by:

$$Z_{cell}(\omega) = j(\omega L_R - \frac{1}{\omega C_L}) \tag{5}$$

$$Y_{cell}(\omega) = j(\omega C_R - \frac{1}{\omega L_L}) \tag{6}$$

Thus, the dispersion relation is written as:

$$\beta(\omega) = s(\omega)\sqrt{\omega^2 L_R C_R + \frac{1}{\omega^2 L_L C_L} - (\frac{L_R}{L_L} + \frac{C_R}{C_L})}, \tag{7}$$

where:

$$s(\omega) = -1,\ if\ \omega < \omega_1 = min(\frac{1}{\sqrt{L_R C_L}}, \frac{1}{\sqrt{L_L C_R}}) \tag{8}$$

or

$$s(\omega) = +1,\ if\ \omega > \omega_2 = max(\frac{1}{\sqrt{L_R C_L}}, \frac{1}{\sqrt{L_L C_R}}) \tag{9}$$

The dispersion curve of this TL is shown in Fig.7. As illustrated, there is a frequency window where the propagation constant is negative (LH regime) and another one where the propagation is RH. A bandgap (between $\omega_1$ and $\omega_2$) separates these two regions. The bandgap can be eliminated by carefully choosing the values for the shunt and series capacitances and inductances of the unit cell. This case is referred as the balanced case, since it provides a smooth transition between the LH and RH regions. This transition occurs at the frequency:

$$\omega_0 = \sqrt[4]{\frac{1}{C_R L_R C_L L_L}} \tag{10}$$

where the propagation constant is zero and thus the guided wavelength becomes infinite. It is important to note that the propagation behavior of a CRLH TL is not purely LH (PLH) in the LH regime or purely RH (PRH) in the RH regime. This is also illustrated in Fig.7, where there is a clear discrepancy between the curves of a PLH and a CRLH TL operating at the LH regime and the same applies for the RH region. More specifically, it is impossible to achieve purely LH propagation characteristics due to parasitic RH inductance and capacitance that are always present. For this reason, the term

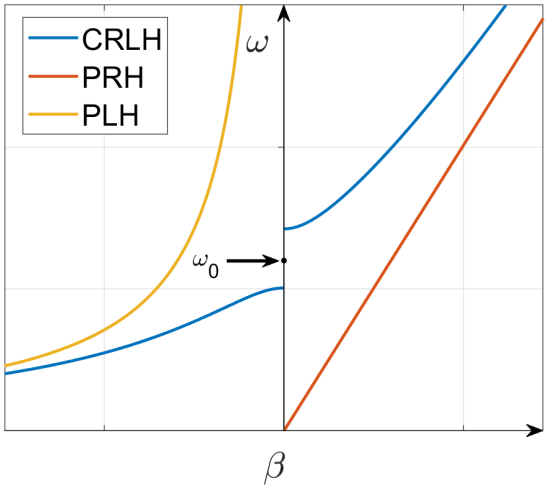


**FIGURE 7.** Dispersion diagrams of a CRLH TL, a purely Left-handed (PLH) TL and a purely Right-handed (PRH) TL.

Composite Right/Left-Handed TL is the most suitable for describing the properties of this line.

From a different point of view, we can equivalently say that a CRLH TL exhibits negative constitutive parameters and thus negative index of refraction in the LH frequency regime. Therefore this type of TL is also referred as negative refractive index (NRI) TL or metamaterial TL, although this terminology is more suitable for 2D and 3D structures that exhibit a metamaterial-like behaviour as it looses its sense when it comes to 1D structures where angles do not have an influence. The effective permittivity and permeability of the CRLH TL for a TEM wave are given by:

$$\epsilon_{eff}(\omega) = L_R - \frac{1}{\omega^2 C_L} \tag{11}$$

$$\mu_{eff}(\omega) = C_R - \frac{1}{\omega^2 L_L} \tag{12}$$

and they are both negative in the LH regime (DNG), one is negative and the other is positive within the bandgap (SNG) and both are positive in the RH region. Regarding the realisation of such a unique medium, it is feasible by periodically loading a conventional RH TL with shunt inductors and series capacitors [31], [32]. An example of a practical implementation based on distributed elements is depicted in Fig.8, where a microstrip line is periodically loaded with interdigital capacitors (series capacitance $C_L$) and grounded stubs (shunt inductance $L_L$). This configuration allows for a more wideband and low-loss metamaterial LH behaviour than a periodic arrangement of SRRs and thin wires, while it is also compatible with other typical microwave components.

Artificial magnetic conductors (AMCs) are surfaces that fully reflect incident waves with a near zero reflection phase ($R_{AMC} \approx 1 + 0j$) and when the loss is neglected they are considered as complementary to perfect electric conductors (PECs), where $R_{PEC} = -1$ [33]. AMCs can be considered as metamaterials, since their unique property cannot be found in

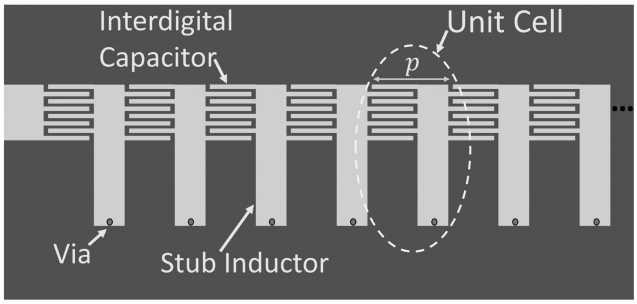


**FIGURE 8.** Practical implementation of CRLH TL with unit cells consisting of interdigital capacitors and stub grounded inductors. The value of *p* is the periodicity of the unit cell and light grey depicts metallization.

conventional materials. The useful bandwidth of an AMC is defined as the frequency interval in which the reflection phase lies between $-90°$ and $+90°$. This definition arises from the fact that within this phase interval the image currents are more in-phase than out-of-phase. AMCs are also referred as high impedance surfaces (HIS), since the magnetic field has small values relative to the electric field's magnitude.

Metal sheets such as ground planes or reflectors are extensively used in antennas in order to direct the wave towards a desired direction. In particular, the distance between the antenna and the metal sheet has to be quarter of the wavelength. Otherwise, the image currents will interfere destructively with the antenna's currents and the radiation efficiency will be poor. On the contrary, the image current due to the presence of an AMC in the proximity of the radiator (i.e. $d \ll \lambda/4$) will not cancel the antenna's currents and the radiation efficiency will be high. In addition, surface waves propagate along the interface of conductors and dielectrics until they reach an edge where they radiate into free space. Therefore, they are considered as the main reason for increased side lobes and distorted radiation patterns. If the metal is replaced with a high impedance structure, the propagation of surface waves is prohibited within a specific bandgap. Hence, AMCs offer an excellent opportunity for low-profile antennas with focused radiation patterns. As far as the realisation of AMC surfaces, they usually consist of periodically arranged metallic patterns of arbitrary shapes printed on a dielectric board [34]–[37]. Some AMC unit cells are depicted in Fig.9.

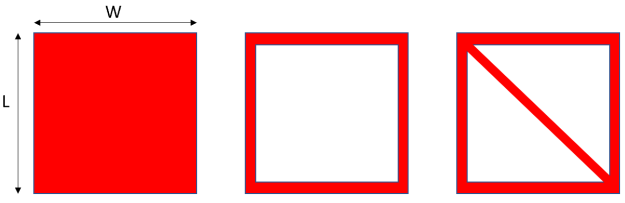


**FIGURE 9.** Different AMC unit cells. Red parts depict conducting material.

It is made clear that in general, metamaterials are structures composed of conducting wires with an arbitrary geometry,

in order to achieve some unique functionality and novel manipulation of electromagnetic waves. Another characteristic is their small size in comparison to the operating wavelength and their low profile, that makes it easy to integrate them with larger microwave components such as antennas.

## III. METAMATERIAL APPLICATIONS

### A. ANTENNA MINIATURISATION

Electrically small antennas (ESAs) have gained great attention due to their small size and low-profile that makes them ideal for several applications such as mobile phones, wearable, airborne and IoT devices. Antennas are considered small when $k\alpha < 1$ or $k\alpha < 0.5$ when no ground is involved. Here, $\alpha$ is the radius of the minimum sphere surrounding the antenna and $k$ is the wave vector for corresponding frequency of operation. Despite the fact that ESAs fulfill the need of compact transceivers, their radiation efficiency $\eta$ and bandwidth are usually degraded [38]. More specifically, a miniaturized antenna is not necessarily an efficient radiator and thus the main challenge is to achieve small size and high performance simultaneously. Traditional miniaturization techniques include the use of lumped elements, shorting pins [39] or high permittivity dielectrics such as ceramic materials [40]. However, these methods result in degraded radiation characteristics. For this reason, metamaterial-based small antennas were introduced to overcome the restrictive limitations and enhance the radiation properties. Before examining the metamaterial-based small antennas and their performance characteristics, it is necessary to gain an insight into some useful definitions and limitations of small antennas. Many authors have explored the fundamental limits of small antennas [41]–[46]. The $Q$ value, which is the ratio of the stored power to the power associated with radiation and losses, is a convenient quantity to describe the bandwidth of an antenna, which is an antenna characteristic of paramount importance in wireless communications. More specifically, the minimum $Q$ for omni-directional antennas is the Chu limit:

$$Q_{min} = \frac{1}{(k\alpha)^3 + k\alpha} \tag{13}$$

and

$$Q_{min} = \frac{1}{2}\left(\frac{1}{(k\alpha)^3} + \frac{2}{k\alpha}\right) \tag{14}$$

for linearly and circularly polarized small antennas respectively. The bandwidth is proportional to the inverse Q-factor ($BW \approx 1/Q$). Consequently, as the electrical length of the antenna decreases, the bandwidth decreases dramatically as well. This indicates that small antennas are more likely to exhibit narrowband performance. In particular, the accomplished bandwidth will achieve the Chu limit, only if the antenna's current distribution sufficiently utilises the minimum sphere that enclosures it. In other words, the antenna geometry should be carefully designed so that the corresponding current distribution results in maximum bandwidth.

Metamaterials and their unique properties are considered as a promising solution for reaching these fundamental limits of small antennas. The following papers investigated and proposed the usage of metamaterials for antenna miniaturisation. In a more theoretical approach, Ziolkowski *et al.* examined the performance of a subwavelength dipole surrounded by a dispersion-less ENG shell [47]. The main idea is that the inductance introduced by the ENG shell compensates for the capacitive nature of the short electric dipole and allows for proper impedance matching of the composite antenna. The initial assumption that the ENG shell is dispersion-less is not realistic but can offer a valuable insight into the general concept. In fact, Veselago in his initial work already pointed out that ENG, MNG and DNG media shall be dispersive in order for the energy of the system to be positive. Nevertheless, the obtained results of this paper showed that designing high-performance electrically small antennas is theoretically feasible, but in the realistic case where the ENG shell exhibits dispersive behaviour, the performance is worsened in comparison to the dispersion-less case. The same author in [48], showed that the bandwidth of antennas consisting of a dipole and ENG shells is highly influenced by the dispersion of the metamaterial while the efficiency is not affected. They demonstrated a system with quality factor that is 2.5 times below the Chu limit. Another interesting theoretical investigation regarding miniaturization of patch antennas with metamaterial loading is presented in [49]. In contrast to prior work [50], [51] that exclusively focused on minimizing the patches dimensions for a certain resonant mode, this paper examined the radiation properties of the modes as well. In other words, they explored the characteristics and the placement of metamaterial loadings not only for shrinking the antenna's dimensions but also for achieving good radiation properties. The authors considered the rectangular patch of Fig.10, which is filled with two different materials, and evaluated the resonant frequencies by applying a standard cavity model. It was shown that arbitrary low resonant frequencies can be obtained independently from the patches dimensions when the permittivities of the two materials have opposite signs. Moreover, it was argued that by properly engineering the materials underneath a circular patch, efficient radiating modes similar to those of regular patches can exist even for smaller dimensions. Hence, simultaneous miniaturization and adequate radiation is theoretically viable.

Another interesting approach for antenna miniaturisation arises from the metamaterial TL approach. It was mentioned previously that a balanced CRLH TL (without a bandgap between the LH and RH regions) exhibits an infinite guided wavelength ($\lambda_g = \infty$) at $\omega_0$ as the propagation constant $\beta(\omega_0)$ becomes zero. This can be translated into an arbitrary antenna size since the resonance frequency is independent of the physical volume and depends only on the LC values of the unit cell. Consequently, a significant size reduction can be achieved. This type of antennas are referred as zeroth-order resonators (ZOR), where the name originates from conventional TL mode numbering. This method was

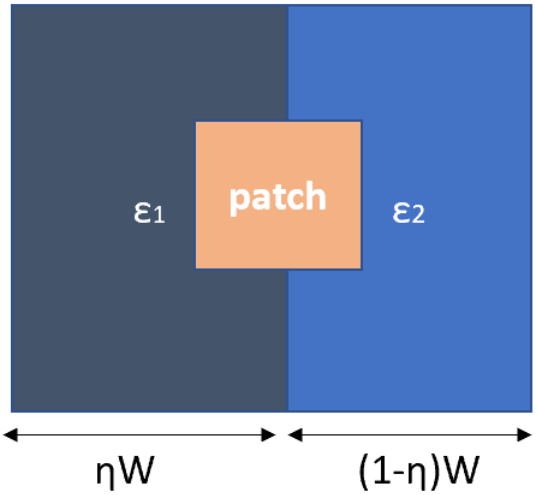


**FIGURE 10.** Patch antenna filled with two different materials [49], which can be SNG, DNG or conventional dielectric.

exploited in [52], where 61% size reduction (in comparison to a conventional resonator) was accomplished by utilizing the cascaded unit cells of Fig. 8. Similarly, an antenna with a length of $\lambda/6$ was proposed in [53] and is shown in Fig. 11. Here, meander-line inductors were introduced for the realization of the shunt inductance.

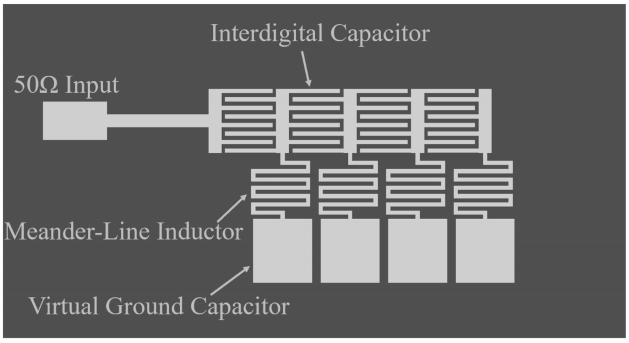


**FIGURE 11.** The planar miniaturized ZOR antenna proposed in [53]. Light grey depicts metallization.

As far as practical designs of metaresonator small antennas, several miniaturized monopole variations were presented in [54] and are shown in Fig.12. According to the authors, the design was straightforward. After they simulated a single SRR unit cell and carefully tuned its geometric parameters to achieve resonance in the desired band, they placed it in the proximity of monopoles with lengths of $\lambda/10 - \lambda/14$. Due to the magnetic coupling between the SRR and the monopoles, the frequency of the composite antennas was shifted towards the SRR's resonance (2.4GHz), while the initial monopole resonance (5.8GHz) was also maintained. As the authors point out, the negative permeability of the single resonator cell cannot be regarded as the main cause of the miniaturisation, since more unit cells are required to

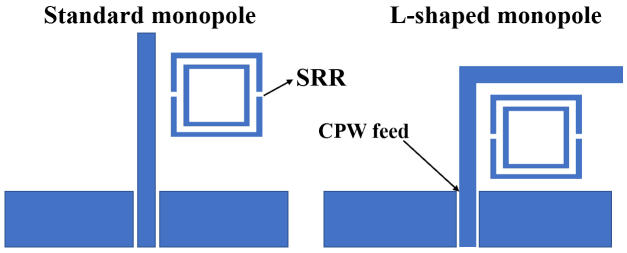


**FIGURE 12.** Miniaturized SRR-based monopole antennas [54].

form an effective medium that has a macroscopical impact. Therefore, the miniaturisation is attributed to the subwavelength resonant nature of the SRR. Moreover, the efficiency and bandwidth of the antennas were acceptable and varied between 0.24 and 0.48 and 30MHz and 127MHz (at 2.4GHz) respectively. In addition, the L-shaped monopole accomplished an efficiency of 0.94, which is remarkable for a small antenna. A similar approach was followed in [55], where electric-LCs (ELC) and their complementary (CELCs) were placed in the proximity of a monopole antenna and resulted in compact size with the efficiency approaching 55%.

In [19], two CSRRs were etched on a standard patch antenna and an AMC surface or RIS (reactive impedance surface) was placed underneath it as illustrated in Fig.13. Here, the authors argued that the CSRR is a high-Q subwavelength resonator but it is not a good radiator since the fields radiated by its slots cancel each other out in the far field and lead to poor efficiency. Therefore, they considered the coupling between the CSRRs (resonant cells with poor radiation) and the patch (non-resonant at the desired frequency but with good radiation) as the key for miniaturisation. In addition, the RIS stores the magnetic energy and increases the inductance of the antenna which results in further frequency decrease. The patches dimensions were $0.099\lambda \times 0.153\lambda$, while the obtained efficiency and gain were 4.7% and $-0.1$dB respectively.

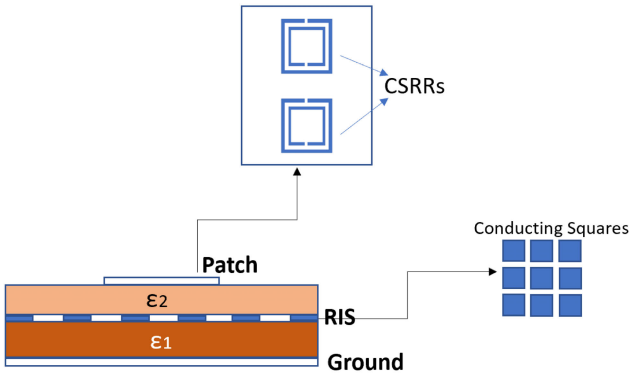


**FIGURE 13.** Small patch antenna with two CSRRs on patch and a RIS underneath [19].

A slightly different approach was followed in [56], where a circular CSRR was placed inside the dielectric substrate

of a circular patch antenna. By using a genetic algorithm, the authors optimized the CSRR's parameters in order to reduce the patches radius to 1/2, 1/3 and 1/4 of the initial one but also maintain acceptable efficiency of 84.7%, 49.8% and 28.1% respectively. The relation between the efficiency and size of the antenna is apparent in this example. Sharawi *et al.* designed a 2 × 2 MIMO antenna platform consisting of small CSRR-based patch antennas [57]. This time the CSRR was etched on the ground plane and resulted in 76% size reduction and 29% efficiency. A dual-band small monopole antenna was presented in [58]. The antenna was loaded with an interdigital capacitor and an inductive slot as shown in Fig.14 and has extremely small dimensions of $1/13.3\lambda_0 \times 1/21.4\lambda_0$ at 2.45GHz. While the unloaded monopole resonates at 5.8GHz, the metamaterial loading (T-shaped slot combined with the interdigital capacitor) forces the currents to wrap around it at 2.4GHz and results in an additional radiating mode at a lower frequency. The measured efficiency at the lower band was 64% and the bandwidth was 90MHz. One of the most efficient miniaturized antennas was designed in [59] and is shown in Fig. 15. The radiating element is a rectangular patch which is fed by a standard microstrip line. A electric-LC (ELC) structure was placed underneath the antenna and tri-band operation (2.5/3.5/5.8 GHz) with over 90% efficiency was achieved while the antenna's footprint was $\lambda/6 \times \lambda/10$.

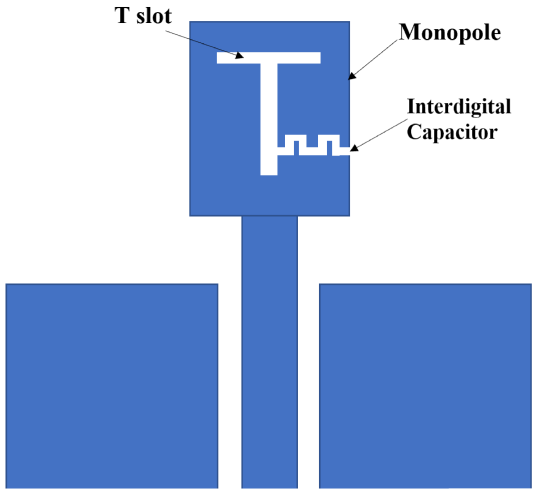


**FIGURE 14.** Small monopole antenna loaded with interdigital capacitor and inductive slot [58].

Another meta-resonator millimeter wave antenna is reported in [60]. Two SRRs were embedded in multilayer LTCC films underneath the radiating patch and the size of the antenna was reduced by 90%. Although the bandwidth and the efficiency are lower in comparison to normal sized antennas, they are acceptable for the majority of applications. In another work, helices instead of SRRs were utilized in [61] to form an MNG medium. This effective MNG medium decreased the size of a circular patch antenna by 60% when it

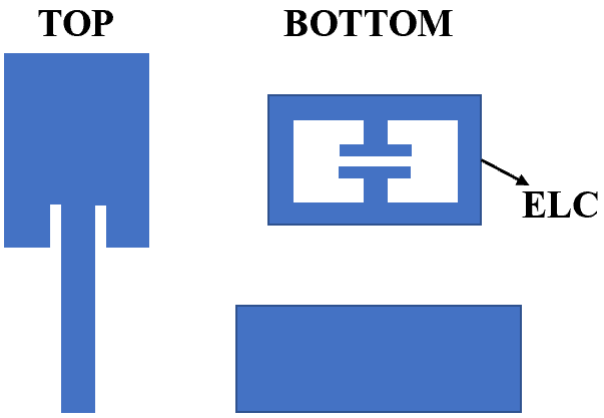


**FIGURE 15.** Small antenna loaded with ELC cell [59].

was placed between the patch and the ground plane. Hence, the theoretical prediction of [49] was verified.

Most of the above presented designs heavily relied on the metaresonator (e.g. SRR, CSRR, ELC) and radiator (e.g. patch, monopole) coupling to accomplish miniaturization. Obviously, a single metaresonator cannot provide negative permittivity or permeability. Therefore, these methods can be considered as equivalent to capacitive and inductive loadings embedded in the antenna structure (which is essentially an RLC resonator) rather than ENG or MNG loadings. This approach is reasonable, since in order to synthesize an effective ENG, MNG or DNG medium, multiple unit cells shall be combined. Thus, there is an immediate increase in size, which is opposed to the goal of these designs [49]. Although metamaterials have gained attention due to their ability of exhibiting negative constitutive parameters, this property is not exploited in most of the designs of small antennas.

From a different point of view, metasurfaces such as AMC and RIS are also utilized for antenna miniaturization. The authors of [75] provide an interesting analysis of AMC surfaces acting as ground planes for planar antennas. By placing a partially reflecting surface (PRS) as superstrate of a radiating element (source) that lies over a ground plane, a Fabry-Perot cavity of height $h$ is created as shown in Fig.16. The ground plane can be either PEC or AMC. The radiation can be described by following the paths of the waves that are reflected multiple times within the cavity. For the radiated power to be maximized, the transmitted waves should be in-phase:

$$\Delta\phi = \phi_2 - \phi_1 = 2N\pi,\ N = 0, 1, 2, \ldots \tag{15}$$

If $\phi_R$, $\phi_G$ denote the phase shift introduced by the PRS and ground plane respectively, the height $h$ can be calculated by:

$$h = \frac{\lambda}{4\pi}(\phi_R + \phi_G) + N\frac{\lambda}{2}, \quad N = 1, 2, \ldots \tag{16}$$

Assuming a highly reflective PRS ($\phi_R = \pi$) and given that $\phi_{PEC} = -\pi$ while $\phi_{PMC} = 0$, we conclude that the minimum

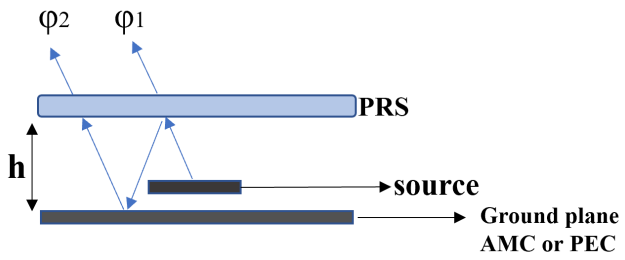


**FIGURE 16.** Fabry-Perot Cavity consisting of an antenna placed between a PRS and a Ground Plane [35].

height is $\lambda/2$ and $\lambda/4$ for a PEC and PMC ground plane. Hence, a significant size reduction for the same radiated power can be accomplished by replacing typical metal sheets with AMC surfaces.

In order to evaluate the performance of the metamaterial-inspired small antennas, we will compare them with a simple patch antenna of high dielectric constant. High values of the substrate's dielectric constant result in smaller patch dimensions for the same frequency of operation [3]. This is a traditional technique for the design of printed antennas with reduced size. Fig.17 shows the patches dimensions for given substrate dielectric and operation at 2.45GHz. We chose the frequency of 2.45GHz since it is a commonly used frequency band and many of the metamaterial antenna designs targeted it as well. As illustrated, the antenna can be as small as 15 mm × 15 mm which corresponds to an electric size of $0.12\lambda \times 0.12\lambda$. The bandwidth of this patch antenna is 2.5% while the efficiency is almost 70%. The radiation pattern resembles the one of standard patch antennas with lower values of dielectric constant but obviously the gain (4.5dBi) is also lower due to the smaller aperture. Such an antenna composed of natural materials has similar or smaller dimensions than most of the metamaterial antennas operating at the same frequency and its corresponding efficiency is high while its design is straightforward. By truncating the corners of such a simple patch, circular polarisation can be achieved. Circular polarisation is a necessary characteristic for many applications (e.g. satellite communications) and challenging to accomplish with metaresonator designs. In fact, only [19] presented a circularly polarized metamaterial antenna. We can conclude that although metamaterial ESAs have a great potential, further investigations and designs that push the frontiers and accelerate the design process are still necessary. Finally, some of the ESA designs presented previously along with their properties are summarized in table 1.

### B. GAIN ENHANCEMENT

Gain is one of the most important antenna characteristics, especially in fixed point-to-point communications and radar systems. Antennas with high gain are able to increase the communication range for a given transmitted power and are more resistant to interference. The directivity of an antenna is proportional to its aperture and thus the deployment of electrically large antennas or antenna arrays with multiple radiating

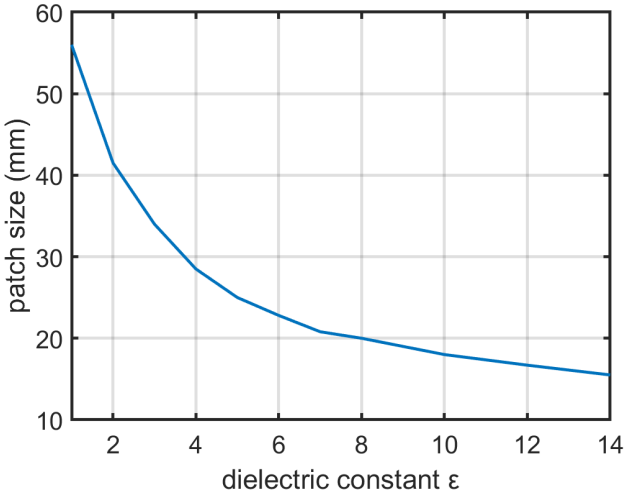


**FIGURE 17.** The dimensions of a square patch for resonance at 2.45GHz vs the dielectric constant of its substrate.

**TABLE 1.** Miniaturized antennas in the literature.

| Reference | Dimensions | Efficiency | Bandwidth |
|---|---|---|---|
| [54] | $\lambda/10 \times \lambda/10$ | 90% | 4.9% |
| [56] | $\lambda/10 \times \lambda/10$ | 28.1% | 0.4% |
| [57] | $\lambda/9 \times \lambda/7$ | 29% | 2% |
| [58] | $\lambda/13.3 \times \lambda/21.4$ | 64% | 3.6% |
| [59] | $\lambda/6 \times \lambda/10$ | 98% | 2.4% |
| [19] | $\lambda/10 \times \lambda/8$ | 22.5% | 1.04% |
| [62] | $\lambda/14 \times \lambda/14$ | 79% | 6.4% |
| [55] | $\lambda/7 \times \lambda/7$ | 55% | 1.55% |

elements are common practices for achieving higher gain [3]. Furthermore, the relation between antenna directivity and size prohibits the usage of small antennas for several applications where high gain is required. It becomes obvious that ultra-compact and high-gain antenna platforms are challenging to implement. As a result, metamaterial radomes superstrates, and lenses have been proposed during the last years as a promising, low-cost alternative for gain increasement without significantly affecting the volume of the antenna. These structures are placed above the radiating element and modify its farfield radiation pattern by interacting with the electromagnetic fields in the vicinity of the radiator. There are two main metamaterial-based techniques that are capable of accomplishing gain enhancement:

- Placement of ZIM (zero-index materials) or NZRI (near-zero refractive index) materials as superstrate.
- Deployment of AMC surfaces in the vicinity of the radiators.
- Placement on GRIN (Gradient Refractive Index) metamaterial lenses in front of the antenna.

NZRI materials have a refractive index $n$ that approaches zero. As illustrated from the dispersion curves of the thin wires and the SRR, there is a narrow window of frequency

where $\epsilon \approx 0$ and $\mu \approx 0$. Hence, materials with $n = \sqrt{\epsilon_{eff}\mu_{eff}} = 0$ can be composed of metamaterial cells that exhibit either zero permittivity or zero permeability at the frequency of operation. Given a metamaterial slab with $n = 0$ and according to the Snell's law, the transmitted wave will be focused perpendicularly to the medium interface regardless of the incidence angle. In particular, Enoch *et al.* demonstrated that the radiation beam of an antenna embedded in a metamaterial will be refracted in a direction very close to the normal when the refractive index of the metamaterial medium is close to zero [63]. This is depicted in Fig.18 and a more detailed analysis can be found in [64] and [65]. This interesting feature of transforming spherical waves into planar can be translated into a gain enhancement when such a medium is used as superstrate or enclosures an antenna. It has also motivated several researchers to investigate its feasibility in practical antenna designs by increasing the effective aperture of the antenna.

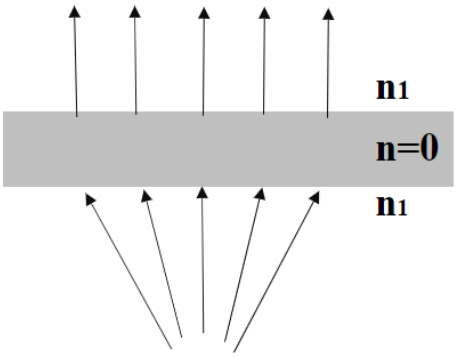


**FIGURE 18.** Transmission through a NZRI slab.

More specifically, a superstrate consisting of metallic square-rings whose two corners are connected with metallic diagonal strips was proposed in [66] and is shown in Fig. 19. The metallic square-rings exhibit zero permittivity at 2.6GHz and this NZRI superstrate was placed at a height of $\lambda/12$ above two microstrip patch antennas operating at the same frequency. The structure was fabricated and the gain of the patches was increased by 3.4dB, while the low-profile of the array was maintained. A layer of similar unit cells with small gaps on the rings was designed in [67] and, according to full wave simulations, increased the gain of a planar antenna by 6.2dB.

In parallel, the authors of [68] proposed a combination of MSRRs (Modified Split-Ring Resonators) and small patches as a metamaterial cell that possesses zero permeability and permittivity simultaneously. The advantage of a superstrate synthesized by these cells is that it can be easier tuned to match to the characteristic impedance of free space. An H-plane horn antenna and a patch antenna were integrated with this zero-index superstrate and a 4.43dB and 6.6dB gain enhancement was observed respectively. By taking advantage of the same principle, a metamaterial lens of S-shaped cells

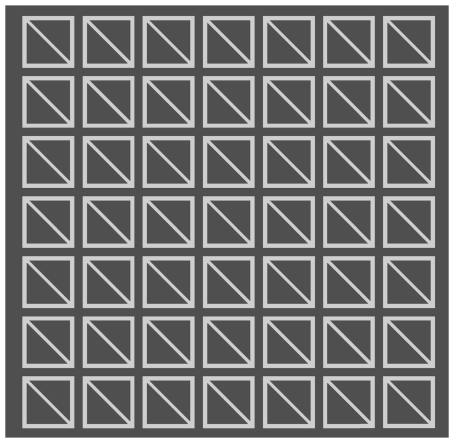

**FIGURE 19.** The NZRI metasurface proposed in [66] for gain enhancement of a patch antenna. Light grey depicts metallization.

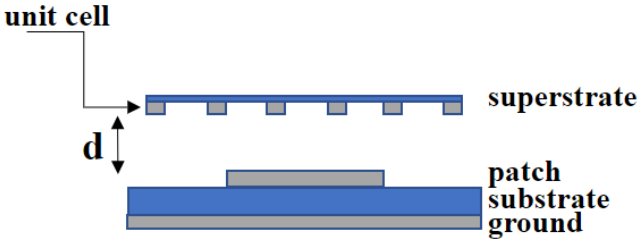


**FIGURE 20.** Superstrate placed above a patch antenna.

with metal strips was designed and fabricated in [69]. The placement of a single lens over a WLAN patch antenna resulted in a 2.05dB increase in gain, while additional 0.6dB enhancement was reported with a double lens. Furthermore, three layers of ELC (Electric Field Coupled) resonators were utilized as a radome of a patch antenna in [70] and the realized gain was 80% of the radiation of a perfect radiating surface with the same area. Hence, the proposed structure accomplished a remarkable 7.8dB gain improvement in comparison to the conventional patch antenna. Zhou *et al.* designed an array of thin metallic patches which exhibits zero index of refraction at 8.75GHz and consequently high directivity of 17.3dB was reported when two of these arrays were placed above a patch antenna [71]. In [72], a circular SRR-based superstrate enhanced the beam focusing of a microstrip antenna by 4dB while the bandwidth was also improved due to the presence of this metasurface. A flat lens in front of a horn antenna resulted in 2dB more gain and highly improved its aperture efficiency [73]. It is worth mentioning that an increase in the gain is not necessarily accompanied by lower side lobes or higher front-to-back ratio. In fact, the superstrate used in [74] led to higher side and back lobes. It follows that if the side and back lobes can be suppressed the gain of the main beam will be further improved.

AMC surfaces have a great potential for gain enhancement and a standard configuration is shown in Fig. 21. A dual-band AMC was designed in [76] and consisted of square patches

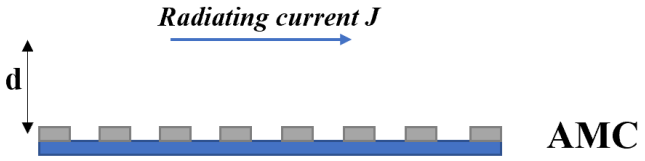


**FIGURE 21.** Standard configuration of radiator placed above an AMC.

with annular slots. The structure was placed at a distance of $\lambda/8$ behind a wideband patch monopole and resulted in a gain enhancement of almost 10dBs while it also performed better than typical PEC reflectors of the same size. Similarly, a fractal AMC was utilized in [77] for performance improvement of a bow-tie antenna and the gain was increased by approximately 4dB. In [78], the authors optimized an electromagnetic band-gap structure (EBG) in order to maximize the frequency window in which wave propagation is prohibited (i.e. imaginary wave number), while such a structure also exhibited a reflection phase response similar to an AMC. Hence, a dipole antenna was improved in terms of reflection coefficient and gain when placed at a distance of 1.5mm from the top of the EBG surface. The gain increased by a maximum of 5.7dB within the operating bandwidth, while contrary to a PEC placed at a same distance from the antenna, the AMC allowed for proper impedance matching.

GRIN (Gradient Index) lenses are known for their ability to focus electromagnetic radiation and transform spherical waves into planar ones. This is accomplished by a gradual variation of the refractive index $n(x, y, z)$, where $x, y, z$ are the cartesian coordinates, that is capable of manipulating and shaping the radiation beam. In this way, the realisation of lenses that do not exhibit the aberration of the conventional lenses (i.e. conventional dielectric lenses which rely on dielectric interfaces) but have equivalent performance is possible. An advantage of GRIN lenses compared to conventional ones is that they can theoretically accomplish wave collimation with arbitrary geometry given a sufficient refractive index profile [79]. Among the most famous refractive index profiles of GRIN lenses are the Luneburg distribution [80]:

$$n(r) = \sqrt{\epsilon_r} = \sqrt{2 - \left(\frac{r}{R}\right)^2}, \quad 0 \le r \le R \tag{17}$$

and the Maxwell's fish-eye distribution:

$$n(r) = \sqrt{\epsilon_r} = \frac{n_0}{1 + \left(\frac{r}{R}\right)^2}, \quad 0 \le r \le R \tag{18}$$

where $R$ is the radius of the lens, $r$ is the distance from any point to the center of the lens and $\epsilon_r$ is the relative permittivity. The distribution of Eq.17 in its discrete form is illustrated in Fig.22 A point source lying on the surface of a Luneburg lens is transformed into a collimated beam on its diametrically opposite side. Meanwhile, Maxwell's fish-eye lens is capable of focusing a point on its surface to the diametrically opposite one, such that a spherical wave at the surface of the lens is converted into a plane wave at the center and is retransformed into a spherical one on the

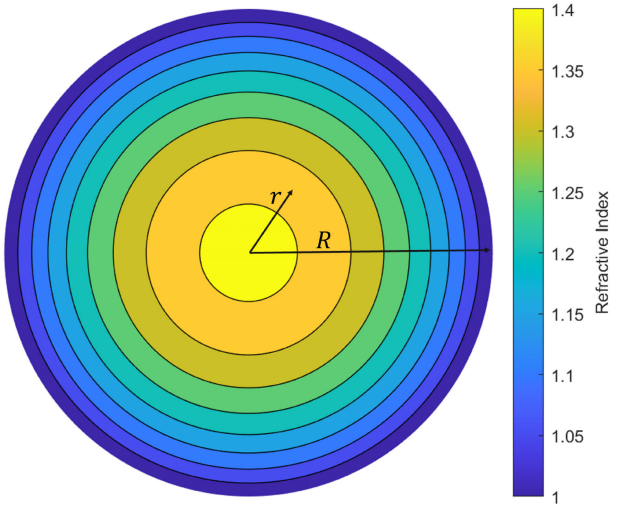


**FIGURE 22.** Gradient refractive index distribution of the cross section of a spherical Luneburg lens. The distribution here is discrete and not continuous, since this is the easiest profile that can be synthesized in practice.

opposite side. Thus for transforming a spherical wavefront to a planar one, usually half Maxwell's fish-eye (hemispherical) lenses are deployed.

The main concern is the feasibility of implementing GRIN lenses with properly engineered refractive index profiles, given that such materials do not exist in nature and should be synthesized in a different way. Hence, an alternative approach for the realisation of GRIN distributions was reported and is based on metamaterials and the ability of alternating their effective refractive index by tuning their geometric parameters [81]. In contrast to the ZIM and NZRI cells, the metamaterials that compose a GRIN lens are being operated at frequencies far away from their resonant frequency. Therefore, their dispersion curves are almost constant in this regime, as shown in Fig.4 and Fig.2 for $\omega \gg \omega_m$ and $\omega \gg \omega_p$ respectively. This means that the effective refractive index of the cells is also constant at these frequencies and changes with small variations in the cell's geometry. A GRIN lens can be synthesized by different layers (meta-layers), where each one of them consists of metamaterial cells that exhibit different index of refraction according to their geometry. With the placement of these layers as in Fig.22, the total distribution approximates the one required for beam collimation. A tremendous advantage of GRIN lenses in comparison to the previous methods is their wide bandwidth and low loss since the metamaterial cells are far from their narrowband resonance and can offer great performance.

The researchers in [82] combined an antipodal vivaldi antenna with a planar GRIN lens consisting of unit cells of three rectangular-shaped metallic strips etched on both sides of a dielectric substrate. Different strip size exhibited different index of refraction that varied between 1.2 to 3.7. A gain enhancement of 9.5dB over a bandwidth of 5GHz was measured after the lens was placed at a distance of $0.38\lambda$

over the vivaldi antenna. A lens composed of thin wires was reported in [83], where several layers were placed in front of a wideband monopole (distance of $\lambda/2$ at the center frequency), thus resulting in an additional gain of 5.3dB. A vivaldi antenna was embedded in a parallel-plate waveguide in order to illuminate a half Maxwell's fish-eye lens [84]. The lens is illustrated in Fig. 23. The spherical waves produced by the vivaldi antenna enter the lens and reemerge as planar ones at its output. The lens consists of complementary square rings, where the refractive index depends on the square's dimensions and thus a gradient profile is created. The proposed antenna accomplished a directivity that is only 1-3dB (over the operational bandwidth) lower compared to an ideal aperture with the same physical dimensions.

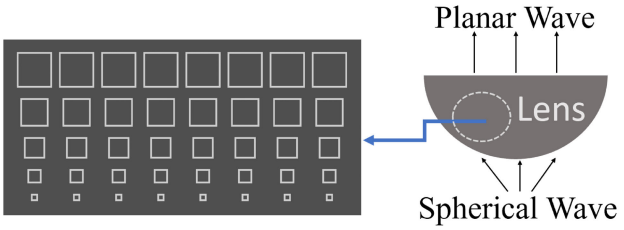


**FIGURE 23.** The half Maxwell's fish-eye lens proposed in [84], where complementary square rings are etched on a thin metallic sheet. The refractive index increases as the dimensions of the squares increase.

Another interesting feature of GRIN lenses is the fact that they can enhance the radiation towards a desired direction regardless of the input wave's incident angle. This characteristic emerges in symmetric lenses and is attractive for beamsteering applications, where the gain has to be high as the steering angle varies and not only towards the boresight direction. This is illustrated in Fig. 24, where the spherical waves of the feed antenna are transformed to planar waves at the output of the GRIN lens independently of the feed's orientation. This has been demonstrated in [85], where a horn antenna was rotated in order to illuminate the GRIN lens from different angles. The gain dropped about 2.5dB for a scan angle of 40°. Planar log periodic dipole antennas (PLPDA) were used as source for a Luneburg lens that was constructed with layers of different dielectric constant [86]. The antennas were placed along the circumference of the lens with different orientations covering the angles from 5° up to 175°. Beam scanning was accomplished by switching between the PLPDA elements (activating one feed at a time), while the lens provided high gain for all directions. Although this lens was not based on metamaterials, it is a great example of the applications of GRIN lenses.

In general, it seems that NZRI superstrates are more suitable for antennas that already have a directive radiation pattern whereas AMC surfaces are more beneficial for transforming omni-directional radiators into directional ones. GRIN lenses have a superior performance in terms of bandwidth and are compatible with beamsteerable antennas as well. In addition, the gain can theoretically remain constant

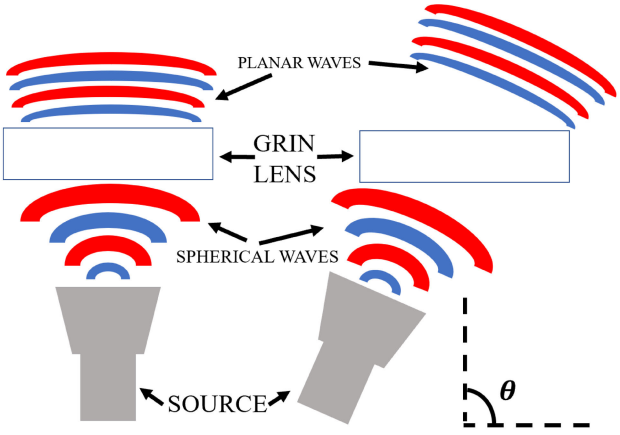


**FIGURE 24.** Illustration of transformation of a spherical wave into a quasi-planar one (through a GRIN lens) for different incident angles $\theta$. This characteristic is attractive for beamsteering applications. Although the lens is depicted as a square for simplicity, it usually has a symmetric shape.

for all steering angles, when a symmetric lens is used. This feature is of great importance and is usually not the case for electronically scanned arrays. Furthermore, they exhibit lower loss as their metamaterial cells are far from their resonance. Their drawback is the increased design complexity in comparison to NZRI and AMC surfaces, since the design and combination of several layers with different properties is required. Finally, some of the works associated with the gain enhancement methods along with the corresponding gain improvement and radiator - metasurface distance are summarized in table 2.

**TABLE 2.** Gain enhancement in the literature.

| Reference | Distance to Radiator | Gain Improvement | Technique |
|---|---|---|---|
| [66] | $\lambda/12$ | 3.4dB | NZRI |
| [67] | $\lambda/2$ | 6.2dB | NRZI |
| [68] | - | 6.6dB | NRZI |
| [69] | $0.55\lambda$ | 2.1dB | NRZI |
| [70] | $0.75\lambda$ | 7.8dB | NRZI |
| [72] | $\lambda/2$ | 4dB | NRZI |
| [76] | $0.4\lambda$ | 10dB | AMC |
| [77] | $\lambda/8$ | 4dB | AMC |
| [78] | $\lambda/40$ | 5.7dB | AMC |
| [82] | $0.38\lambda$ | 9.5dB | GRIN |
| [83] | $\lambda/2$ | 5.3dB | GRIN |

### C. ISOLATION

Isolation is of great importance for innumerous applications, in which the antenna elements are placed in close proximity either due to the system's design (e.g. typical $\lambda/2$ interelement spacing in antenna array configurations) or for minimizing the structure's volume. As a result, crosstalk

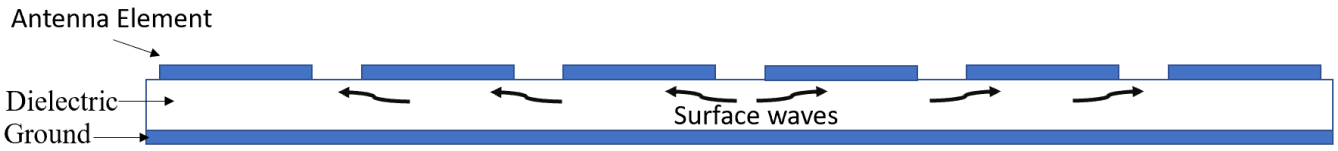


**FIGURE 25.** Illustration of coupling due to surface waves in multi-antenna platforms.

arises because of the electromagnetic coupling between the antennas. In particular for planar antennas that are printed on the same board, surface waves are regarded as the main source of crosstalk. Surface waves are TE or TM modes that propagate along the antenna's substrate and get diffracted on the air-dielectric interface [87]. The cut-off frequencies of the modes are given by:

$$f_c = \frac{nc}{4h\sqrt{\epsilon_r - 1}} \tag{19}$$

where $n = 1, 3, \ldots$ for TE, $n = 0, 2, \ldots$ for TM, $h$ and $\epsilon_r$ are the substrate's height and relative permittivity respectively. It is clear that the $TM_0$ is always excited and it is not possible to prohibit its propagation with proper substrate design. This is also illustrated in Fig.25. Furthermore, some applications for which decoupling of antennas and suppression of surface waves are required for optimum performance are the following:

- **Repeaters:** Isolation between the transmitter and receiver of a repeater is necessary for protecting the amplifier that enhances the desired signal from saturation [88].
- **Radars:** The sensitivity of FMCW radars is severely affected by the phase noise that is included in the transmitter's signal which leaks into the receiver. The phase noise is usually of sufficient magnitude compared to the target's echo and thus the SNR is significantly decreased unless the transmitter and receiver modules are adequately decoupled [89].
- **MIMO:** Here, mutual coupling between antenna elements increases the correlation of the received signals and thus is detrimental to the channel capacity [90].
- **Beamforming:** Interelement coupling in densely-packed antenna arrays results in radiation pattern distortion that degrades the beamsteering [91].

Prior art concerning isolation includes i) placement of parasitic elements which create a reverse coupling [92], ii) polarization diversity [93], iii) decoupling networks and grounds [94]–[96], iv) increased distance between the transmit and receive antennas [99] or placement of metal sheets between them [97], [98]. Under certain circumstances, these methods have proven to be effective for isolation enhancement but also lead in high complexity, increased volume and are limited to specific applications. Several metamaterial decoupling structures have been proposed as an alternative to the previously mentioned techniques. Emphasis is mainly placed on isolation enhancement in planar antenna topologies, since they are low-profile and suitable for most of the applications but also suffer from high coupling due to the excitation of surface waves and space waves.

More specifically, a compact MIMO platform consisting of two printed monopoles operating at 2.4GHz was examined in [100]. The platform is shown in Fig. 26. The distance between the two antennas was $\lambda/8$ and thus the coupling between them ($S21$ and $S12$ coefficients) has a high value of -5dB. The authors proposed an easy to fabricate and efficient solution. They first examined the electric field of the structure, in order to find the path through which the power flows from one antenna to the other. After this, they placed a capacitive-loaded split rectangular loop (CLSRL) [101], exactly at the point where the power flow is maximum. In this manner, more than 30dB coupling reduction was accomplished.

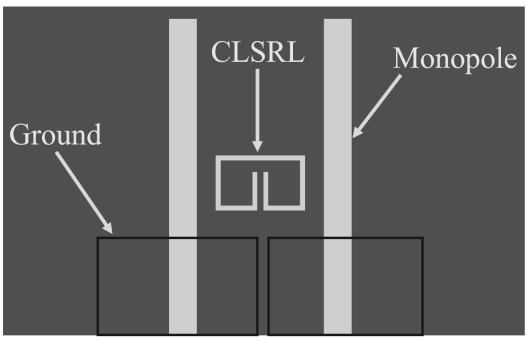


**FIGURE 26.** Decoupling of two closely spaced monopole antennas with a single metamaterial CLSRL unit cell [100]. Light grey depicts metallization and the ground plane (black outline) is placed underneath the substrate (dark grey).

Furthermore, two meander-like structures were placed between two closely spaced patch antennas in [102]. The resonators provided an isolation improvement of 16dB at 4.5GHz. A Mu-negative isolation technique for densely packed monopoles was proposed in [103]. The authors considered this metamaterial-structure as a filter, that decouples the antennas over the whole operational bandwidth. In a similar manner, SRR inclusion pairs were inserted between monopoles in [104] and resulted in 25dB coupling reduction, while the impedance matching of the antennas was not affected. A four-element isolation enhancement of 42dB was presented in [105], where a mushroom-like structure was utilized. The authors of [106] presented a systematic approach for a dual-band metasurface design that significantly decreases the coupling between two adjacent elements in two frequency bands (2.6 GHz, 3.5 GHz). The metasurface

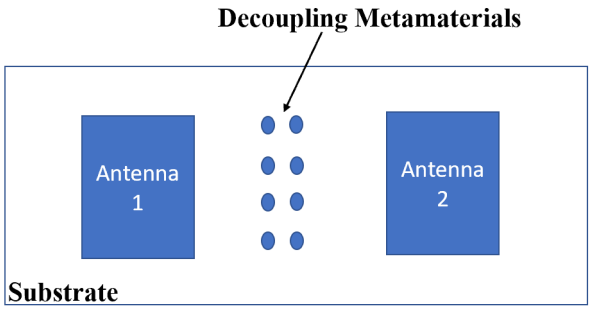


**FIGURE 27.** Standard configuration of isolation enhancement with metamaterials placed between two closely spaced antennas.

layer consists of double layer cut wires of different lengths and is placed above the antennas as a superstrate. A similar decoupling mechanism was proven to be effective in [107], where a SRR-based superstrate offered wideband isolation ($S21 < -27dB$), while the volume of the structure was not dramatically increased.

Moreover, dual-band (2.34-2.47GHz, 3.35-3.65GHz) isolation improvement was presented from the authors of [108]. After they designed an electrically small CSRR-based antenna, they placed two of those in proximity (e.g. edge-to-edge spacing of 10 mm. For the decoupling, they utilized a $2 \times 3$ array of modified CSRRs (called CSR2) that exhibit a bandgap in the corresponding frequencies and thus resulted in coupling reduction in both bands. Excellent decoupling at the 28GHz 5G band was reported in [109]. Three CSRRs connected with extra slots were inserted between the elements and adequately decreased the coupling by 27dB. The authors used the theory of the characteristics mode to optimise the CSRR structure in order to act as a band-rejection filter. It was observed that by connecting the CSRRs with slots the stopband response had wider bandwidth and offered better isolation. In [110], a flower-shaped metamaterial cell was designed to exhibit high absorptivity at 5.5GHz. By placing an array of these cells between two closely spaced patch antennas, the coupling was reduced by 12.41dB. The authors report also 4% higher efficiency due to the higher isolation. A fractal metamaterial was utilized in [111] and offered wideband decoupling at five frequency bands without degrading the radiation pattern or the efficiency. Hence, it is a promising candidate for multi-band isolation.

Reconfigurable and tunable metamaterials are a novel concept that combines the benefits of metamaterials with the adaptivity of tunable elements such as varactors and MEMS [112]–[114]. Such a structure was utilized in [115] for adaptive decoupling of closely spaced antennas. A screen consisting of many varactor-based metaresonators was introduced between the antennas and thus the response of the structure could be manipulated by applying proper voltages on each unit cell. Since it is impossible to derive an analytical solution, a genetic algorithm was applied to optimize the isolation by finding the corresponding voltages of each unit cell. In this manner, a remarkable coupling reduction was accomplished with $S21 = -120$dB. On another note, a phased array consisting of patch antennas operating at 5.6 GHz was presented in [116]. A metamaterial slab acting as a wall is placed between adjacent H-plane elements and significantly reduced the mutual coupling by almost 20dB. Consequently, an overall performance improvement was noticed with smoother radiation pattern and eliminated scan blindness. In addition, the metawall was composed of modified SRRs that exhibit low loss and thus the efficiency was not mitigated. Moreover, a MIMO system with enhanced isolation is reported in [117]. The proposed unit cell in this case is a meander-like structure where one part of the metalization is a bit elevated (3D) and connected with short cylinders to the rest of the body. This structure reduced the coupling of adjacent elements with an edge-to-edge spacing of $0.13\lambda_0$ by 18dB.

Finally, some of the works presented are summarized in table 3, while the methodology for isolation enhancement of antennas is the following:

**TABLE 3.** Isolation in the literature.

| Reference | Method | Element distance | Isolation enhancement |
|---|---|---|---|
| [100] | CLSRL | $\lambda/8$ | 30dB |
| [102] | Meanders | $\lambda/9$ | 16dB |
| [103] | CLSRL | $\lambda/9$ | 30dB |
| [104] | SRR | $\lambda/8$ | 45dB |
| [105] | Mushroom | $\lambda/2$ | 16dB |
| [106] | Wires | $0.008\lambda$ | 25dB |
| [107] | SRR superstrate | $0.02\lambda$ | 19dB |
| [108] | CSRR | $0.08\lambda$ | 15dB |
| [117] | 3D cell | $0.13\lambda$ | 18dB |

**1.)** Find the position/s where the power flow from one antenna to the other is maximum for the given frequency of operation. In particular for printed antennas, observe the power flow within the substrate.

**2.)** Examine the electric and magnetic field vectors at the position where the power flow is maximized, when only one antenna is excited. This will highly depend on the antenna's radiation characteristics (e.g. standard monopoles/patches create well-known electric and magnetic field polarisations).

**3.)** Choose a metamaterial unit cell that can operate under the presence of the electric and magnetic fields observed in the previous step. For instance, SRRs are excited by magnetic fields perpendicular to their axis, while CSRRs are excited from electric fields. Optimize the unit cell's parameters for resonance at the desired frequency and minimum magnitude of the permittivity's and permeability's imaginary part. The latter is important for reducing the loss which is directly related to the imaginary part of the constitutive parameters. This analysis can be carried systemically with the techniques presented in [118], a full wave simulator and an

optimisation algorithm or a simple parametric sweep. For example, the simulation setup for the extraction of a CSRR's parameters is illustrated in Fig.28. The boundary conditions PEC (Perfect Electric Conductor) and PMC (Perfect Magnetic Conductor) are utilized to simulate an incident plane wave with the electric field being perpendicular to the CSRR's axis.

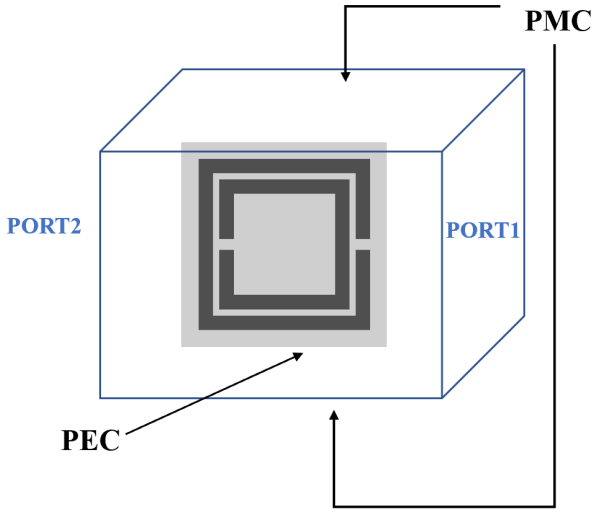


**FIGURE 28.** Simulation Setup of a single CSRR until cell. Light grey depicts metalization.

**4.)** Place the optimized metamaterial cells at the position of maximum power flow. It should be pointed out that the isolation improves with an increase in the number of the metamaterial cells but the efficiency is usually degraded due to higher energy storage and losses caused by additional cells.

## IV. DISCUSSION AND FUTURE CHALLENGES

### A. METAMATERIAL ESA CHALLENGES

In several works the antenna dimensions were considerably reduced and the structures were remarkably small in comparison to the wavelength. Since ESAs exhibit limitations, their design is challenging and requires compromises between antenna size and performance (i.e. bandwidth, efficiency). Although metamaterials proved to be effective in reducing the size of the radiators by enabling novel resonant modes (i.e. ZOR antennas), the main challenges remain unchanged. For instance, the narrowband nature of metamaterials directly affects the bandwidth of the small metaresonator antennas. In addition, most of the designs focused exclusively on reducing the size by leveraging the subwavelength resonance of metamaterial cells, but the overall antenna performance was not optimized. In particular, the interaction between the metamaterial cell and the rest of the antenna (e.g. monopole, patch) was not taken into account, despite the fact that this interaction is rather crucial for the current distribution that highly determines the antenna performance. Designing an ESA with a metaresonator loading can be straightforward, but accomplishing an overall good performance requires further design considerations such as feeding mechanism, metamaterial type, position of the unit cell/s, shape of the main antenna body, etc. Hence, we conclude that metamaterials accelerate and assist the design of ESAs, but further investigations are needed.

In addition, there is a great necessity for theoretical formulations that will act as design guidelines in order for the antenna characteristics to be optimized. Clearly, the field is not mature yet and although there are some great examples of metamaterial antennas, the scientific insight into the working principles is limited and the designs mainly rely on EM simulations. Hence, the formulation of a solid theory behind metamaterial-inspired antennas that will accelerate the design process and ultimately benefit the performance is necessary. In particular, techniques for improving the narrow bandwidth and low efficiency of ESAs with metamaterials are of great importance for future communications. As the bandwidths become larger, the devices more compact and SNR is the dominant parameter for the upcoming 5G and beyond networks, small, power-efficient and wideband antennas will be a vital component.

### B. GAIN

Gain depends on two main parameters: aperture efficiency and size. Various NZRI superstrates and AMC surfaces have been proposed for gain improvement with the former having the ability of focusing electromagnetic power on a single point and the latter acting as reflectors or forming cavities. Metamaterial-inspired GRIN lenses have also been reported and provided increased gain over a wide bandwidth. Unarguably, the corresponding gain increase of these methods is mainly attributed to the increase in aperture size (i.e. superstrates, lenses and reflectors have larger dimensions than the radiators). Nevertheless, they also offer higher aperture efficiency and can be placed closer to the antennas than conventional reflectors. In addition, such surfaces are cheaper and easier to fabricate than metallic reflectors that require extreme surface smoothness in higher frequencies. In particular, metamaterials are an excellent alternative for the realization of gradient index profiles that are traditionally implemented by combining different dielectric layers. On the other hand, the NRZI and AMC based gain enhancement techniques have only been applied to fixed-beam antennas and their integration with beamsteerable antennas has not been examined yet. This arises from the fact that AMC and NRZI superstrates focus the radiation towards a specific direction. For simultaneous gain enhancement and beamsteering to be viable, the metamaterial radomes shall be reconfigurable so that they adapt to the changes and increase the directivity regardless of the main beam's direction. Only GRIN lenses have been integrated with beamsteerable antennas, where the system relies either on mechanical rotation of the feed antenna or switching between elements with different orientation. This is rather uncomfortable as there is a necessity for electronically controlled/scanned antenna systems that have the benefits of being faster and adaptive. Furthermore, this kind of GRIN

lenses are usually not planar and thus somewhat unsuitable for many applications where a low profile is required. Since beamforming is a key technology in modern wireless communications, an increase in gain for any given beam direction will further increase the performance and result in even higher SNR at the receiver. Hence, adaptive NRZI and AMC metasurfaces and low-profile metamaterial GRIN lenses for gain enhancement of beamsteerable arrays are an interesting research topic.

### C. ISOLATION

Regarding metamaterial-based isolation, the electrodynamics of SNG and DNG media can offer a solid understanding of the working principles. Here, metamaterials offer an excellent alternative and are a smart, low-profile solution for adequate decoupling. In fact, they nor increase the size and neither significantly affect the antenna characteristics. Despite the fact that the levels of the achieved isolation are considered sufficient for several applications, the corresponding bandwidth is limited. This is again attributed to the narrowband metamaterial response. As a result, it is challenging to decouple wideband antennas with the proposed methods. Apart from this, metamaterial isolation of multi-band antennas is also exigent, since most of the metamaterial insulators operate at a single frequency. Hence, there is a clear antithesis to the ever increasing bandwidth and multiple frequency operation of modern communication systems. In addition, most of the works discussed here, consider a single horizontally arranged pair of antennas. This is opposed once again to the demands of modern and future technologies such as massive MIMO, where a large number of antennas in various configurations is required. As a result, we identify a clear necessity for wideband/multi-band isolation solutions for multi-antenna systems that have arbitrary antenna topologies.

In parallel, most of the works regarding isolation have focused on antennas for communication systems, where the specifications are less strict (i.e. usually $-20$dB for MIMO arrays). Radars are more demanding and require as high transmitter-receiver isolation as possible. Hence, metamaterial solutions that provide extreme levels of isolation (e.g below $-100$dB) are necessary for improving radar performance and maintaining a low profile by avoiding the placement of large metal sheets between the transmitter and the receiver.

## V. CONCLUSION

This article presented a detailed review of antennas inspired by metamaterial principles and highlighted their strengths and weaknesses. A brief introduction in the theory of metamaterials provided an insight into their novel properties and capabilities. Electrically small antennas, antenna gain and isolation enhancement with metamaterials were discussed in detail and an overview of the state-of-the-art was also presented. The design tradeoffs considerations and methodologies show that metamaterials offer exciting new opportunities for future wireless communications and radar systems. Their unique characteristics offer design techniques that were not applicable in the past but can be realized today though many design challenges are yet to be addressed as discussed in this review.

As a final note, we are of the view that more designs should be studied in order for the field to become mature and for metamaterial-inspired antennas to have an active role in future wireless communications thus penetrating into the global market. They can certainly contribute to the new era of enhanced connectivity and power efficiency. Finally, we believe that this review can serve as an inspiration and reference point in further developing metamaterial antennas to enable wide-ranging applications.

## REFERENCES

[1] A. J. Paulraj, D. A. Gore, R. U. Nabar, and H. Bolcskei, "An overview of MIMO communications—A key to gigabit wireless," *Proc. IEEE*, vol. 92, no. 2, pp. 198–218, Feb. 2004.

[2] S. M. Razavizadeh, M. Ahn, and I. Lee, "Three-dimensional beamforming: A new enabling technology for 5G wireless networks," *IEEE Signal Process. Mag.*, vol. 31, no. 6, pp. 94–101, Nov. 2014.

[3] C. A. Balanis, *Antenna Theory: Analysis and Design*. Hoboken, NJ, USA: Wiley, 2016.

[4] M. O. Akinsolu, K. K. Mistry, B. Liu, P. I. Lazaridis, and P. Excell, "Machine learning-assisted antenna design optimization: A review and the state-of-the-art," in *Proc. 14th Eur. Conf. Antennas Propag. (EuCAP)*, Copenhagen, Denmark, Mar. 2020, pp. 1–5.

[5] V. Grout, M. O. Akinsolu, B. Liu, P. I. Lazaridis, K. K. Mistry, and Z. D. Zaharis, "Software solutions for antenna design exploration: A comparison of packages, tools, techniques, and algorithms for various design challenges," *IEEE Antennas Propag. Mag.*, vol. 61, no. 3, pp. 48–59, Jun. 2019.

[6] F. Tariq, M. R. A. Khandaker, K.-K. Wong, M. A. Imran, M. Bennis, and M. Debbah, "A speculative study on 6G," *IEEE Wireless Commun.*, vol. 27, no. 4, pp. 118–125, Aug. 2020.

[7] D. R. Smith, O. Yurduseven, L. P. Mancera, P. Bowen, and N. B. Kundtz, "Analysis of a waveguide-fed metasurface antenna," *Phys. Rev. A, Gen. Phys.*, vol. 8, no. 5, pp. 1–16, Nov. 2017.

[8] M. Lin, X. Huang, B. Deng, J. Zhang, D. Guan, D. Yu, and Y. Qin, "A high-efficiency reconfigurable element for dynamic metasurface antenna," *IEEE Access*, vol. 8, pp. 87446–87455, 2020.

[9] M. Alibakhshikenari, F. Babaeian, B. S. Virdee, S. Aissa, L. Azpilicueta, C. H. See, A. A. Althuwayb, I. Huynen, R. A. Abd-Alhameed, F. Falcone, and E. Limiti, "A comprehensive survey on various decoupling mechanisms with focus on metamaterial and metasurface principles applicable to SAR and MIMO antenna systems," *IEEE Access*, vol. 8, pp. 192965–193004, 2020.

[10] P. Kumar, T. Ali, and M. M. M. Pai, "Electromagnetic metamaterials: A new paradigm of antenna design," *IEEE Access*, vol. 9, pp. 18722–18751, 2021.

[11] A. Alu, N. Engheta, A. Erentok, and R. W. Ziolkowski, "Single-negative, double-negative, and low-index metamaterials and their electromagnetic applications," *IEEE Antennas Propag. Mag.*, vol. 49, no. 1, pp. 23–36, Feb. 2007.

[12] V. G. Veselago, "The electrodynamics of substances with simultaneously negative values of $\epsilon$ and $\mu$," *Soviet Phys. Uspekhi*, vol. 10, pp. 509–514, Apr. 1968.

[13] J. B. Pendry, A. J. Holden, W. J. Stewart, and I. Youngs, "Extremely low frequency plasmons in metallic mesostructures," *Phys. Rev. Lett.*, vol. 76, no. 25, pp. 4773–4776, Jun. 1996.

[14] J. B. Pendry, A. J. Holden, D. J. Robbins, and W. J. Stewart, "Magnetism from conductors and enhanced nonlinear phenomena," *IEEE Trans. Microw. Theory Techn.*, vol. 47, no. 11, pp. 2075–2081, Nov. 1999.

[15] A. Marwaha, "An accurate approach of mathematical modeling of SRR and SR for metamaterials," *J. Eng. Sci. Technol. Rev.*, vol. 9, no. 6, pp. 82–86, Dec. 2016.

[16] M. Shamonin, E. Shamonina, V. Kalinin, and L. Solymar, "Properties of a metamaterial element: Analytical solutions and numerical simulations for a singly split double ring," *J. Appl. Phys.*, vol. 95, no. 7, pp. 3778–3784, Apr. 2004.
[17] S. S. Karthikeyan and R. S. Kshetrimayum, "Composite right/left handed transmission line based on open slot split ring resonator," *Microw. Opt. Technol. Lett.*, vol. 52, no. 8, pp. 1729–1731, Aug. 2010.
[18] J. Naqui and F. Martín, "Application of broadside-coupled split ring resonator (BC-SRR) loaded transmission lines to the design of rotary encoders for space applications," in *IEEE MTT-S Int. Microw. Symp. Dig.*, San Francisco, CA, USA, May 2016, pp. 1–4.
[19] Y. Dong, H. Toyao, and T. Itoh, "Design and characterization of miniaturized patch antennas loaded with complementary split-ring resonators," *IEEE Trans. Antennas Propag.*, vol. 60, no. 2, pp. 772–785, Feb. 2012.
[20] F. Falcone, T. Lopetegi, M. A. G. Laso, J. D. Baena, J. Bonache, M. Beruete, R. Marqués, F. Martín, and M. Sorolla, "Babinet principle applied to the design of metasurfaces and metamaterials," *Phys. Rev. Lett.*, vol. 93, no. 19, Nov. 2004, Art. no. 197401.
[21] R. Marqués, F. Mesa, J. Martel, and F. Medina, "Comparative analysis of edge- and broadside-coupled split ring resonators for metamaterial design—Theory and experiments," *IEEE Trans. Antennas Propag.*, vol. 51, no. 10, pp. 2572–2581, Oct. 2003.
[22] J. D. Baena, J. Bonache, F. Martín, R. M. Sillero, F. Falcone, T. Lopetegi, M. A. G. Laso, J. Garcia-Garcia, I. Gil, M. F. Portillo, and M. Sorolla, "Equivalent-circuit models for split-ring resonators and complementary split-ring resonators coupled to planar transmission lines," *IEEE Trans. Microw. Theory Techn.*, vol. 53, no. 4, pp. 1451–1461, Apr. 2005.
[23] F. Zhang, G. Houzet, E. Lheurette, D. Lippens, M. Chaubet, and X. Zhao, "Negative-zero-positive metamaterial with omega-type metal inclusions," *J. Appl. Phys.*, vol. 103, no. 8, Apr. 2008, Art. no. 084312.
[24] H. Chen, L. Ran, J. Huangfu, X. Zhang, K. Chen, T. M. Grzegorczyk, and J. A. Kong, "Negative refraction of a combined double S-shaped metamaterial," *Appl. Phys. Lett.*, vol. 86, no. 15, Apr. 2005, Art. no. 151909.
[25] T. H. Hand, J. Gollub, S. Sajuyigbe, D. R. Smith, and S. A. Cummer, "Characterization of complementary electric field coupled resonant surfaces," *Appl. Phys. Lett.*, vol. 93, no. 21, Nov. 2008, Art. no. 212504.
[26] D. R. Smith, W. J. Padilla, D. C. Vier, S. C. Nemat-Nasser, and S. Schultz, "Composite medium with simultaneously negative permeability and permittivity," *Phys. Rev. Lett.*, vol. 84, no. 18, pp. 4184–4187, May 2000.
[27] A. K. Iyer and G. V. Eleftheriades, "Negative refractive index metamaterials supporting 2-D waves," in *IEEE MTT-S Int. Microw. Symp. Dig.*, San Antonio, TX, USA, vol. 2, Jun. 2002, pp. 1067–1070.
[28] C. Caloz and T. Itoh, "Application of the transmission line theory of left-handed (LH) materials to the realization of a microstrip LH line," in *Proc. IEEE AP-S Int. Symp.*, San Antonio, TX, USA, vol. 1, Jun. 2002, pp. 412–415.
[29] A. A. Oliner, "A periodic-structure negative-refractive-index medium without resonant elements," in *Proc. USNC/URSI Nat. Radio Sci. Meeting*, San Antonio, TX, USA, Jun. 2002, p. 41.
[30] C. Caloz and T. Itoh, *Electromagnetic Metamaterials Transmission Line Theory and Microwave Applications*. New York, NY, USA: Wiley, 2006.
[31] C. Caloz and T. Itoh, "Transmission line approach of left-handed (LH) materials and microstrip implementation of an artificial LH transmission line," *IEEE Trans. Antennas Propag.*, vol. 52, no. 5, pp. 1159–1166, May 2004.
[32] G. V. Eleftheriades, A. K. Iyer, and P. C. Kremer, "Planar negative refractive index media using periodically L-C loaded transmission lines," *IEEE Trans. Microw. Theory Techn.*, vol. 50, no. 12, pp. 2702–2712, Dec. 2002.
[33] D. Sievenpiper, L. Zhang, R. F. J. Broas, N. G. Alexopolous, and E. Yablonovitch, "High-impedance electromagnetic surfaces with a forbidden frequency band," *IEEE Trans. Microw. Theory Techn.*, vol. 47, no. 11, pp. 2059–2074, Nov. 1999.
[34] Y. Zheng, J. Gao, X. Cao, Z. Yuan, and H. Yang, "Wideband RCS reduction of a microstrip antenna using artificial magnetic conductor structures," *IEEE Antennas Wireless Propag. Lett.*, vol. 14, pp. 1582–1585, 2015.
[35] A. Foroozesh and L. Shafai, "Investigation into the application of artificial magnetic conductors to bandwidth broadening, gain enhancement and beam shaping of low profile and conventional monopole antennas," *IEEE Trans. Antennas Propag.*, vol. 59, no. 1, pp. 4–20, Jan. 2011.
[36] M. E. de Cos, Y. Alvarez, and F. Las-Heras, "Novel broadband artificial magnetic conductor with hexagonal unit cell," *IEEE Antennas Wireless Propag. Lett.*, vol. 10, pp. 615–618, 2011.
[37] R. C. Hadarig, M. E. de Cos, and F. Las-Heras, "Novel miniaturized artificial magnetic conductor," *IEEE Antennas Wireless Propag. Lett.*, vol. 12, pp. 174–177, 2013.
[38] L. J. Volakis, C.-C. Chen, and K. Fujimoto, *Small Antennas: Miniaturization Techniques and Applications*. New York, NY, USA: McGraw-Hill, 2010.
[39] R. Porath, "Theory of miniaturized shorting-post microstrip antennas," *IEEE Trans. Antennas Propag.*, vol. 48, no. 1, pp. 41–47, Jan. 2000.
[40] J. Kula, D. Psychoudakis, W.-J. Liao, C.-C. Chen, J. Volakis, and J. Halloran, "Patch-antenna miniaturization using recently available ceramic substrates," *IEEE Antennas Propag. Mag.*, vol. 48, no. 6, pp. 13–20, Dec. 2006.
[41] L. J. Chu, "Physical limitations of omnidirectional antennas," *J. Appl. Phys.*, vol. 19, pp. 1163–1175, Dec. 1948.
[42] H. A. Wheeler, "Fundamental limitations of small antennas," *Proc. IRE*, vol. 35, no. 12, pp. 1479–1484, Dec. 1947.
[43] R. P. Harrington, *Time Harmonic Electromagnetic Fields*. New York, NY, USA: McGraw-Hill, 1961, pp. 414–420.
[44] R. Collin and S. Rothschild, "Evaluation of antenna Q," *IEEE Trans. Antennas Propag.*, vol. AP-12, no. 1, pp. 23–27, Jan. 1964.
[45] R. C. Hansen, "Fundamental limitations in antennas," *Proc. IEEE*, vol. 69, no. 2, pp. 170–181, Feb. 1981.
[46] J. S. McLean, "A re-examination of the fundamental limits on the radiation Q of electrically small antennas," *IEEE Trans. Antennas Propag.*, vol. 44, no. 5, pp. 672–676, May 1996.
[47] R. W. Ziolkowski and A. Erentok, "Metamaterial-based efficient electrically small antennas," *IEEE Trans. Antennas Propag.*, vol. 54, no. 7, pp. 2113–2130, Jul. 2006.
[48] R. W. Ziolkowski and A. Erentok, "At and below the Chu limit: Passive and active broad bandwidth metamaterial-based electrically small antennas," *IET Microw., Antennas Propag.*, vol. 1, no. 1, pp. 116–128, Feb. 2007.
[49] A. Alù, F. Bilotti, N. Engheta, and L. Vegni, "Subwavelength, compact, resonant patch antennas loaded with metamaterials," *IEEE Trans. Antennas Propag.*, vol. 55, no. 1, pp. 13–25, Jan. 2007.
[50] J. S. Petko and D. H. Werner, "Theoretical formulation for an electrically small microstrip patch antenna loaded with negative index materials," in *Proc. IEEE AP-S USNC/URSI Int. Symp.*, Washington, DC, USA, Jul. 2005, pp. 343–346.
[51] M. E. Ermutlu and S. Tretyakov, "Patch antennas partially loaded with a dispersive backward-wave material," in *Proc. IEEE Antennas Propag. Soc. Int. Symp.*, Washington, DC, USA, Jul. 2005, pp. 6–9.
[52] A. Sanada, C. Caloz, and T. Itoh, "Zeroth order resonance in composite right/left-handed transmission line resonators," in *Proc. Asia–Pacific Microw. Conf.*, Seoul, South Korea, vol. 3, Nov. 2003, pp. 1588–1591.
[53] A. Sanada, M. Kimura, I. Awai, C. Caloz, and T. Itoh, "A planar zeroth-order resonator antenna using a left-handed transmission line," in *Proc. 34th Eur. Microw. Conf.*, vol. 3, Apr. 2005, pp. 1341–1344.
[54] D. K. Ntaikos, N. K. Bourgis, and T. V. Yioultsis, "Metamaterial-based electrically small multiband planar monopole antennas," *IEEE Antennas Wireless Propag. Lett.*, vol. 10, pp. 963–966, 2011.
[55] H. Odabasi, F. L. Teixeira, and D. O. Guney, "Electrically small, complementary electric-field-coupled resonator antennas," *J. Appl. Phys.*, vol. 113, no. 8, Feb. 2013, Art. no. 084903.
[56] R. O. Ouedraogo, E. J. Rothwell, A. R. Diaz, K. Fuchi, and A. Temme, "Miniaturization of patch antennas using a metamaterial-inspired technique," *IEEE Trans. Antennas Propag.*, vol. 60, no. 5, pp. 2175–2182, May 2012.
[57] M. S. Sharawi, M. U. Khan, A. B. Numan, and D. N. Aloi, "A CSRR loaded MIMO antenna system for ISM band operation," *IEEE Trans. Antennas Propag.*, vol. 61, no. 8, pp. 4265–4274, Aug. 2013.
[58] J. Zhu and G. V. Eleftheriades, "Dual-band metamaterial-inspired small monopole antenna for WiFi applications," *Electron. Lett.*, vol. 45, no. 22, pp. 1104–1106, Oct. 2009.
[59] K. Li, C. Zhu, L. Li, Y.-M. Cai, and C.-H. Liang, "Design of electrically small metamaterial antenna with ELC and EBG loading," *IEEE Antennas Wireless Propag. Lett.*, vol. 12, pp. 678–681, 2013.
[60] I. K. Kim and V. V. Varadan, "Electrically small, millimeter wave dual band meta-resonator antennas," *IEEE Trans. Antennas Propag.*, vol. 58, no. 11, pp. 3458–3463, Nov. 2010.
[61] S. Jahani, J. Rashed-Mohassel, and M. Shahabadi, "Miniaturization of circular patch antennas using MNG metamaterials," *IEEE Antennas Wireless Propag. Lett.*, vol. 9, pp. 1194–1196, 2010.

[62] N. K. Bourgis and T. V. Yioultsis, "Efficient isolation between electrically small metamaterial-inspired monopole antennas," *Prog. Electromagn. Res. B*, vol. 60, pp. 227–239, Aug. 2014.
[63] S. Enoch, G. Tayeb, P. Sabouroux, N. Guérin, and P. Vincent, "A metamaterial for directive emission," *Phys. Rev. Lett.*, vol. 89, no. 21, Nov. 2002, Art. no. 213902.
[64] A. Alù, M. G. Silveirinha, A. Salandrino, and N. Engheta, "Epsilon-near-zero metamaterials and electromagnetic sources: Tailoring the radiation phase pattern," *Phys. Rev. B, Condens. Matter*, vol. 75, no. 15, Apr. 2007, Art. no. 155410.
[65] R. W. Ziolkowski, "Propagation in and scattering from a matched metamaterial having a zero index of refraction," *Phys. Rev. E, Stat. Phys. Plasmas Fluids Relat. Interdiscip. Top.*, vol. 70, no. 4, Oct. 2004, Art. no. 046608.
[66] P. K. Panda and D. Ghosh, "Isolation and gain enhancement of patch antennas using EMNZ superstrate," *AEU-Int. J. Electron. Commun.*, vol. 86, pp. 164–170, Mar. 2018.
[67] G. Augustin, B. P. Chacko, and T. A. Denidni, "A zero-index metamaterial unit-cell for antenna gain enhancement," in *Proc. IEEE Antennas Propag. Soc. Int. Symp. (APSURSI)*, Orlando, FL, USA, Jul. 2013, pp. 126–127.
[68] Y. L. Meng, F. Y. Zhang, L. Zhu, J. H. Fu, K. Zhang, and Q. Wu, "A zero index metamaterial lens for gain enhancement of patch antenna and H-plane horn antenna," in *Proc. IEEE Int. Wireless Symp. (IWS)*, Apr. 2013, pp. 1–4.
[69] H. Suthar, D. Sarkar, K. Saurav, and K. V. Srivastava, "Gain enhancement of microstrip patch antenna using near-zero index metamaterial (NZIM) lens," in *Proc. 21st Nat. Conf. Commun. (NCC)*, Feb. 2015, pp. 1–6.
[70] D. Li, Z. Szabo, X. Qing, E.-P. Li, and Z. N. Chen, "A high gain antenna with an optimized metamaterial inspired superstrate," *IEEE Trans. Antennas Propag.*, vol. 60, no. 12, pp. 6018–6023, Dec. 2012.
[71] H. Zhou, Z. Pei, S. Qu, S. Zhang, J. Wang, Z. Duan, H. Ma, and Z. Xu, "A novel high-directivity microstrip patch antenna based on zero-index metamaterial," *IEEE Antennas Wireless Propag. Lett.*, vol. 8, pp. 538–541, 2009.
[72] F. Z. Khoutar, M. Aznabet, and O. E. Mrabet, "Gain and directivity enhancement of a rectangular microstrip patch antenna using a single layer metamaterial superstrate," in *Proc. 6th Int. Conf. Multimedia Comput. Syst. (ICMCS)*, May 2018, pp. 1–4.
[73] Q. Wu, P. Pan, F.-Y. Meng, L.-W. Li, and J. Wu, "A novel flat lens horn antenna designed based on zero refraction principle of metamaterials," *Appl. Phys. A, Solids Surf.*, vol. 87, no. 2, pp. 151–156, Mar. 2007.
[74] H. A. Majid, M. K. A. Rahim, and T. Masri, "Microstrip antenna's gain enhancement using left-handed metamaterial structure," *Prog. Electromagn. Res. M*, vol. 8, pp. 235–247, Jan. 2009.
[75] A. P. Feresidis, G. Goussetis, S. Wang, and J. C. Vardaxoglou, "Artificial magnetic conductor surfaces and their application to low-profile high-gain planar antennas," *IEEE Trans. Antennas Propag.*, vol. 53, no. 1, pp. 209–215, Jan. 2005.
[76] P. Prakash, M. P. Abegaonkar, A. Basu, and S. K. Koul, "Gain enhancement of a CPW-fed monopole antenna using polarization-insensitive AMC structure," *IEEE Antennas Wireless Propag. Lett.*, vol. 12, pp. 1315–1318, 2013.
[77] Y. Zhong, G. Yang, and L. Zhong, "Gain enhancement of bow-tie antenna using fractal wideband artificial magnetic conductor ground," *Electron. Lett.*, vol. 51, no. 4, pp. 315–317, Feb. 2015.
[78] S. D. Assimonis, T. V. Yioultsis, and C. S. Antonopoulos, "Design and optimization of uniplanar EBG structures for low profile antenna applications and mutual coupling reduction," *IEEE Trans. Antennas Propag.*, vol. 60, no. 10, pp. 4944–4949, Oct. 2012.
[79] J. B. Pendry, D. Schurig, and D. R. Smith, "Controlling electromagnetic fields," *Science*, vol. 312, no. 5781, pp. 1780–1782, 2006. [Online]. Available: http://science.sciencemag.org/content/312/5781/1780
[80] R. K. Luneburg and M. Herzberger, *Mathematical Theory of Optics*. Berkeley, CA, USA: Univ. California Press, 1964.
[81] D. R. Smith, J. J. Mock, A. F. Starr, and D. Schurig, "Gradient index metamaterials," *Phys. Rev. E, Stat. Phys. Plasmas Fluids Relat. Interdiscip. Top.*, vol. 71, no. 3, Mar. 2005, Art. no. 036609.
[82] E. Erfani, M. Niroo-Jazi, and S. Tatu, "A high-gain broadband gradient refractive index metasurface lens antenna," *IEEE Trans. Antennas Propag.*, vol. 64, no. 5, pp. 1968–1973, May 2016.
[83] R. Singha and D. Vakula, "Directive beam of the monopole antenna using broadband gradient refractive index metamaterial for ultra-wideband application," *IEEE Access*, vol. 5, pp. 9757–9763, 2017.
[84] A. Dhouibi, S. N. Burokur, A. de Lustrac, and A. Priou, "Low-profile substrate-integrated lens antenna using metamaterials," *IEEE Antennas Wireless Propag. Lett.*, vol. 12, pp. 43–46, 2013.
[85] D. Jia, Y. He, N. Ding, J. Zhou, B. Du, and W. Zhang, "Beam-steering flat lens antenna based on multilayer gradient index metamaterials," *IEEE Antennas Wireless Propag. Lett.*, vol. 17, no. 8, pp. 1510–1514, Aug. 2018.
[86] M. K. Saleem, H. Vettikaladi, M. A. S. Alkanhal, and M. Himdi, "Lens antenna for wide angle beam scanning at 79 GHz for automotive short range radar applications," *IEEE Trans. Antennas Propag.*, vol. 65, no. 4, pp. 2041–2046, Apr. 2017.
[87] R. Garg, P. Bhartia, I. J. Bahl, and A. Ittipiboon, *Microstrip Antenna Design Handbook*. Norwood, MA, USA: Artech House, 2001.
[88] A. G. Dimitriou, "Design, analysis, and performance evaluation of a UHF RFID forward-link repeater," *IEEE J. Radio Freq. Identificat.*, vol. 4, no. 2, pp. 73–82, Jun. 2020.
[89] C. Baktir, E. Sobaci, and A. Dönmez, "A guide to reduce the phase noise effect in FMCW radars," in *Proc. IEEE Radar Conf.*, Atlanta, GA, USA, May 2012, pp. 0236–0239.
[90] P. N. Fletcher, M. Dean, and A. R. Nix, "Mutual coupling in multi-element array antennas and its influence on MIMO channel capacity," *Electron. Lett.*, vol. 39, no. 4, pp. 342–344, Feb. 2003.
[91] A. M. Wyglinski and S. D. Blostein, "On uplink CDMA cell capacity: Mutual coupling and scattering effects on beamforming," *IEEE Trans. Veh. Technol.*, vol. 52, no. 2, pp. 289–304, Mar. 2003.
[92] Z. Li, Z. Du, M. Takahashi, K. Saito, and K. Ito, "Reducing mutual coupling of MIMO antennas with parasitic elements for mobile terminals," *IEEE Trans. Antennas Propag.*, vol. 60, no. 2, pp. 473–481, Feb. 2012.
[93] H. Li, B. K. Lau, Z. Ying, and S. He, "Decoupling of multiple antennas in terminals with chassis excitation using polarization diversity, angle diversity and current control," *IEEE Trans. Antennas Propag.*, vol. 60, no. 12, pp. 5947–5957, Dec. 2012.
[94] L. Zhao, L. K. Yeung, and K.-L. Wu, "A coupled resonator decoupling network for two-element compact antenna arrays in mobile terminals," *IEEE Trans. Antennas Propag.*, vol. 62, no. 5, pp. 2767–2776, May 2014.
[95] S. Zhang, X. Chen, and G. F. Pedersen, "Mutual coupling suppression with decoupling ground for massive MIMO antenna arrays," *IEEE Trans. Veh. Technol.*, vol. 68, no. 8, pp. 7273–7282, Aug. 2019.
[96] Y.-M. Zhang, S. Zhang, J.-L. Li, and G. F. Pedersen, "A transmission-line-based decoupling method for MIMO antenna arrays," *IEEE Trans. Antennas Propag.*, vol. 67, no. 5, pp. 3117–3131, May 2019.
[97] F.-Y. Kuo and R.-B. Hwang, "High-isolation X-band marine radar antenna design," *IEEE Trans. Antennas Propag.*, vol. 62, no. 5, pp. 2331–2337, May 2014.
[98] M. W. Niaz and R. A. Bhatti, "High-isolation antenna system for X-band synthetic aperture radar," *Wireless Pers. Commun.*, vol. 97, no. 2, pp. 2741–2750, Nov. 2017.
[99] D.-H. Shin, D.-H. Jung, D.-C. Kim, J.-W. Ham, and S.-O. Park, "A distributed FMCW radar system based on fiber-optic links for small drone detection," *IEEE Trans. Instrum. Meas.*, vol. 66, no. 2, pp. 340–347, Feb. 2017.
[100] D. A Ketzaki and T. V. Yioultsis, "Metamaterial-based design of planar compact MIMO monopoles," *IEEE Trans. Antennas Propag.*, vol. 61, no. 5, pp. 2758-2766, May 2013.
[101] Y. Guo, G. Goussetis, A. P. Feresidis, and J. C. Vardaxoglou, "Efficient modeling of novel uniplanar left-handed metamaterials," *IEEE Trans. Microw. Theory Techn.*, vol. 53, no. 4, pp. 1462–1468, Apr. 2005.
[102] M. G. N. Alsath, M. Kanagasabai, and B. Balasubramanian, "Implementation of slotted meander-line resonators for isolation enhancement in microstrip patch antenna arrays," *IEEE Antennas Wireless Propag. Lett.*, vol. 12, pp. 15–18, 2013.
[103] S. R. Thummaluru and R. K. Chaudhary, "Mu-negative metamaterial filter-based isolation technique for MIMO antennas," *Electron. Lett.*, vol. 53, no. 10, pp. 644–646, May 2017.
[104] M. M. Bait-Suwailam, M. S. Boybay, and O. M. Ramahi, "Electromagnetic coupling reduction in high-profile monopole antennas using single-negative magnetic metamaterials for MIMO applications," *IEEE Trans. Antennas Propag.*, vol. 58, no. 9, pp. 2894–2902, Sep. 2010.
[105] G. Zhai, Z. N. Chen, and X. Qing, "Enhanced isolation of a closely spaced four-element MIMO antenna system using metamaterial mushroom," *IEEE Trans. Antennas Propag.*, vol. 63, no. 8, pp. 3362–3370, Aug. 2015.

[106] F. Liu, J. Guo, L. Zhao, G.-L. Huang, Y. Li, and Y. Yin, "Dual-band metasurface-based decoupling method for two closely packed dual-band antennas," *IEEE Trans. Antennas Propag.*, vol. 68, no. 1, pp. 552–557, Jan. 2020.
[107] Z. Wang, L. Zhao, Y. Cai, S. Zheng, and Y. Yin, "A meta-surface antenna array decoupling (MAAD) method for mutual coupling reduction in a MIMO antenna system," *Sci. Rep.*, vol. 8, no. 1, Feb. 2018, Art. no. 3152.
[108] A. K. Panda, S. S. Sahu, and R. K. Mishra, "A compact dual-band 2 × 1 metamaterial inspired MIMO antenna system with high port isolation for LTE and WiMax applications," *Int. J. RF Microw. Comput.-Aided Eng.*, vol. 27, no. 8, pp. 1–11, 2017.
[109] A. Abdelaziz and E. K. I. Hamad, "Isolation enhancement of 5G multiple-input multiple-output microstrip patch antenna using metamaterials and the theory of characteristic modes," *Int. J. RF Microw. Comput.-Aided Eng.*, vol. 30, no. 11, Nov. 2020, Art. no. e22416.
[110] P. Garg and P. Jain, "Isolation improvement of MIMO antenna using a novel flower shaped metamaterial absorber at 5.5 GHz WiMAX band," *IEEE Trans. Circuits Syst. II, Exp. Briefs*, vol. 67, no. 4, pp. 675–679, Apr. 2020.
[111] M. Alibakhshikenari, M. Khalily, B. S. Virdee, C. H. See, R. A. Abd-Alhameed, and E. Limiti, "Mutual coupling suppression between two closely placed microstrip patches using EM-bandgap metamaterial fractal loading," *IEEE Access*, vol. 7, pp. 23606–23614, 2019.
[112] G. Oliveri, D. H. Werner, and A. Massa, "Reconfigurable electromagnetics through metamaterials—A review," *Proc. IEEE*, vol. 103, no. 7, pp. 1034–1056, Jul. 2015.
[113] T. Ali, S. Pathan, and R. C. Biradar, "Multiband, frequency reconfigurable, and metamaterial antennas design techniques: Present and future research directions," *Internet Technol. Lett.*, vol. 1, no. 6, p. e19, Nov. 2018.
[114] J. P. Turpin, J. A. Bossard, K. L. Morgan, D. H. Werner, and P. L. Werner, "Reconfigurable and tunable metamaterials: A review of the theory and applications," *Int. J. Antennas Propag.*, vol. 2014, pp. 1–18, May 2014.
[115] L. Zhang, S. Zhang, Z. Song, Y. Liu, L. Ye, and Q. H. Liu, "Adaptive decoupling using tunable metamaterials," *IEEE Trans. Microw. Theory Techn.*, vol. 64, no. 9, pp. 2730–2739, Sep. 2016.
[116] M.-C. Tang, S. Xiao, B. Wang, J. Guan, and T. Deng, "Improved performance of a microstrip phased array using broadband and ultra-low-loss metamaterial slabs," *IEEE Antennas Propag. Mag.*, vol. 53, no. 6, pp. 31–41, Dec. 2011.
[117] K. Yu, Y. Li, and X. Liu, "Mutual coupling reduction of a MIMO antenna array using 3-D novel meta-material structures," *Appl. Comput. Electromagn. Soc. J.*, vol. 33, no. 7, pp. 758–763, 2018.
[118] A. B. Numan and M. S. Sharawi, "Extraction of material parameters for metamaterials using a full-wave simulator [education column]," *IEEE Antennas Propag. Mag.*, vol. 55, no. 5, pp. 202–211, Oct. 2013.

**CHRISTOS MILIAS** was born in Drama, Greece, in 1997. He received the M.Sc. degree in electrical and computer engineering from the Aristotle University of Thessaloniki, Thessaloniki, Greece, in 2020. He is currently pursuing the Ph.D. degree with MyDefence ApS, Nørresundby, Denmark, and the Department of Business and Technology (BTECH), Aarhus University, Denmark. His research interests include antennas and propagation, metamaterials, and radar systems.

**RASMUS B. ANDERSEN** received the M.S. degree in advanced radio frequency design from Aalborg University, Denmark, in 2001. He has worked in the telecommunication industry, since 2001, implementing RF systems from antenna to software defined baseband. From 2011 to 2016, he worked as the Project Manager of organic photovoltaics at Mekoprint and joined MyDefence, in 2016, as a Senior Hardware Engineer, with focus on drone RF sensors, electronic counter measures, and radar sensing. He has headed projects in the fields of product development, commercial-academic collaboration, MIL-STD and medical approvals, and process control and application engineering.

**PAVLOS I. LAZARIDIS** (Senior Member, IEEE) received the M.Eng. degree in electrical engineering from the Aristotle University of Thessaloniki, Greece, in 1990, the M.Sc. degree in electronics from Université Pierre and Marie Curie (Paris 6), Paris, France, in 1992, and the Ph.D. degree from the École Nationale Supérieure des Télécommunications (ENST) Paris and Université Paris 6, in 1996. From 1991 to 1996, he was involved in research at France Télécom, and teaching at ENST Paris. In 1997, he became the Head of the Antennas and Propagation Laboratory, Télédiffusion de France/the France Télécom Research Center (TDF–C2R Metz). From 1998 to 2002, he was a Senior Examiner with the European Patent Office (EPO), The Hague, The Netherlands. From 2002 to 2014, he was involved in teaching and research with the ATEI of Thessaloniki, Greece, and Brunel University, London, U.K. He is currently a Professor of electronics and telecommunications with the University of Huddersfield, U.K. He has been involved in several international research projects, such as EU Horizon 2020 MOTOR5G and RECOMBINE, NATO-SfP ORCA, and he has published over 150 research articles and several national and European patents. He is a member of the IET (MIET), Senior Member of URSI, and a fellow of the Higher Education Academy (FHEA), and is serving as an Associate Editor for IEEE Access.

**ZAHARIAS D. ZAHARIS** (Senior Member, IEEE) received the B.Sc. degree in physics, the M.Sc. degree in electronics, the Ph.D. degree in antennas and propagation modeling for mobile communications, and the Diploma degree in electrical and computer engineering from the Aristotle University of Thessaloniki, Thessaloniki, Greece, in 1987, 1994, 2000, and 2011, respectively. From 2002 to 2013, he was with the Administration of the Telecommunications Network, Aristotle University of Thessaloniki. Since 2013, he has been with the Department of Electrical and Computer Engineering, Aristotle University of Thessaloniki. His current research interests include design and optimization of antennas and microwave circuits, signal processing on smart antennas, development of evolutionary optimization algorithms, and neural networks. He is currently a member of the Technical Chamber of Greece. He is serving as an Associate Editor for IEEE Access.

**BILAL MUHAMMAD** received the Ph.D. degree in telecommunication engineering from the University of Rome Tor Vergata, Italy. He currently works as an Assistant Professor with the Department of Business Development and Technology (BTECH), Aarhus University, Denmark. He actively participates in EU projects and has been a WP leader for SARA and EASY-PV projects funded under H2020 Innovation Action program. His research interests include UAV wireless communication for 5G and Beyond, GNSS integrity and accuracy for UAV, unmanned traffic management (UTM) systems and services, multi-business model innovation, and prototyping UAV applications.

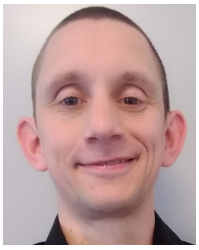

**JES T. B. KRISTENSEN** received the M.Sc. degree in electrical engineering from Aalborg University, Denmark, in 2008, with a specialization in applied signal processing and implementation. From 2008 to 2014, he worked at Rohde & Schwarz (TCDK–Aalborg/Denmark and Munich), as an FPGA and Baseband Developer for WCDMA L1 testing for the CRTU and CMW500 products. Additionally, he worked as a Technical Consultant for starting and facilitating the TD-SCDMA development with R&S China and the Beijing Universities. Since 2014, he has been working at MyDefence (http://mydefence.dk, Denmark), as a Signal Processing Engineer and a General Architect for C-UAV sensors. Defining the core of the RF-sensors and radars in the company portfolio–the Wingman-products, Watchdog-products, Wolfpack- products, and Eagle-products. In addition, he serves as a SCRUM master, a process enthusiast, and an *ad hoc* Technical Project Lead for tenders, research, product development, and the EU KNOX Horizon 2020 Project. LinkedIn: https://www.linkedin.com/in/jestoftkristensen/

**ALBENA MIHOVSKA** (Member, IEEE) received the Ph.D. degree in mobile communications from Aalborg University, Denmark. Since 2017, she has been an Associate Professor with the Department of Business Development and Technology, Aarhus University, Denmark, where she is leading the research activities of the 6G Knowledge Laboratory, with a focus on 6G connectivity and enabling technologies, namely artificial intelligence, and advanced services and applications, such as augmented and extended reality (AR and XR), high-fidelity and real time mobile hologram, and digital twins. She is currently a Senior Research and Academic Professional. She has more than 150 scientific publications.

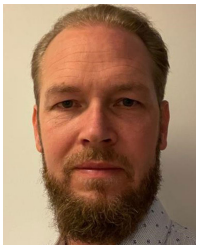

**DAN D. S. HERMANSEN** received the M.Sc. degree in RF engineering and CMOS IC design from Aalborg University, Denmark, in 2005. He has worked in the telecommunication industry for over 20 years on RF related systems and technologies. In 2013, he co-founded MyDefence, which works with security related applications, like anti-drone equipment, including RF sensors, RF jammers, radars, and data fusion. MyDefence has completed numerous research projects within the EU, such as H2020, and Danish Defence and Innovation Fund Denmark Research Programmes, where he has headed the projects.